Molecular Biology of the Cell
Vol. 18, 1203–1219, April 2007

Avl9p, a Member of a Novel Protein Superfamily, Functions in the Late Secretory Pathway[D]

Edina Harsay*† and Randy Schekman†

*Department of Molecular Biosciences, University of Kansas, Lawrence, KS 66045; and †Department of Molecular and Cell Biology, Howard Hughes Medical Institute, University of California, Berkeley, CA 94720

Submitted November 22, 2006; Revised December 29, 2006; Accepted January 10, 2007
Monitoring Editor: Benjamin Glick

The branching of exocytic transport routes in both yeast and mammalian cells has complicated studies of the late secretory pathway, and the mechanisms involved in exocytic cargo sorting and exit from the Golgi and endosomes are not well understood. Because cargo can be sorted away from a blocked route and secreted by an alternate route, mutants defective in only one route do not exhibit a strong secretory phenotype and are therefore difficult to isolate. In a genetic screen designed to isolate such mutants, we identified a novel conserved protein, Avl9p, the absence of which conferred lethality in a *vps1*Δ *apl2*Δ strain background (lacking a dynamin and an adaptor-protein complex 1 subunit). Depletion of Avl9p in this strain resulted in secretory defects as well as accumulation of Golgi-like membranes. The triple mutant also had a depolarized actin cytoskeleton and defects in polarized secretion. Overexpression of Avl9p in wild-type cells resulted in vesicle accumulation and a post-Golgi defect in secretion. Phylogenetic analysis indicated evolutionary relationships between Avl9p and regulators of membrane traffic and actin function.

INTRODUCTION

Membrane vesicle–mediated intracellular transport of proteins and lipids is a fundamental process in all eukaryotic cells. Membrane transport pathways are essential for cell growth and division as well as for maintaining normal cell homeostasis of nondividing cells. The mechanisms of transport carrier formation and fusion of these carriers with their target membranes are well conserved among eukaryotes, so relatively simple organisms can serve as useful models for studying these processes. The yeast *Saccharomyces cerevisiae* has proven to be an especially valuable tool in the study of membrane traffic, and the majority of the components of the secretory machinery shared by all eukaryotic cells were originally identified in yeast (Novick *et al.*, 1980; Bankaitis *et al.*, 1986; Rothman and Stevens, 1986; Robinson *et al.*, 1988).

The first extensive yeast genetic screen for mutants that block the exocytic pathway identified many of the components involved in endoplasmic reticulum-to-Golgi transport and vesicle fusion with the plasma membrane, but only 2 of the 23 genes identified in this screen blocked anterograde transport from the Golgi (Novick *et al.*, 1980; Guo *et al.*, 2000; Lee *et al.*, 2004). As in mammalian cells, there are multiple exocytic transport routes from the yeast Golgi, so cargo in a blocked pathway can be missorted and secreted by an alternate route (Harsay and Bretscher, 1995; Harsay and Schekman, 2002). This has made it difficult to identify mutants that have a defect in exocytic transport from the Golgi, and relatively little is known about the molecular machinery involved at this transport step.

Although small (~40–100 nm) vesicles are the best-characterized transport intermediates in the secretory pathway, larger tubular structures also transport cargo. In mammalian cells, tubular vesicles appear to be the most abundant class of exocytic carriers from the Golgi (Hirschberg *et al.*, 1998; Toomre *et al.*, 1999; Polishchuk *et al.*, 2000; Puertollano *et al.*, 2003). Exocytic vesicles in yeast are smaller but they are formed by some of the same processes, which include elaborate mechanisms that regulate membrane lipid composition at the *trans*-Golgi network (TGN). These involve lipid modifying enzymes such as phospholipase D (Chen *et al.*, 1997; McDermott *et al.*, 2004) and phosphatidylinositol (PtdIns) kinases and phosphatases (Simonsen *et al.*, 2001; Roth, 2004); PtdIns transporter proteins (Bankaitis *et al.*, 1990; Litvak *et al.*, 2005); and aminophospholipid translocases (Chen *et al.*, 1999; Natarajan *et al.*, 2004). The Ras-type small GTPase Arf1 is both a regulator of, and regulated by, the membrane lipid–modifying processes and is a key control factor in transport from the Golgi and endosomes (Nie *et al.*, 2003; D'Souza-Schorey and Chavrier, 2006).

Numerous vesicle coat complexes are involved in recruiting cargo and deforming membranes for vesicle formation. Clathrin-coated vesicles were identified first and are the best characterized transport intermediates (Pearse and Robinson, 1990; Kirchhausen, 2000). Clathrin is linked to membranes by adaptor proteins (APs), which are recruited to donor membranes by cargo proteins, Arf, and specific phosphoinositides (Ghosh and Kornfeld, 2004; Robinson, 2004). Of the various transport vesicle species formed at the TGN, the AP-1 (adaptor protein complex 1)-containing clathrin-coated vesicles may mediate transport to endosomes en route to

This article was published online ahead of print in *MBC in Press* (http://www.molbiolcell.org/cgi/doi/10.1091/mbc.E06–11–1035) on January 17, 2007.

[D] The online version of this article contains supplemental material at *MBC Online* (http://www.molbiolcell.org).

Address correspondence to: Edina Harsay (harsay@ku.edu).

Abbreviations used: AP, adaptor protein; AVL, AP-1 Vps1 Lethal; AH, Avl9 homology; ANR, Avl Nine Related; CSM, complete synthetic medium; DENN, differentially expressed in normal versus neoplastic; HMM, Hidden Markov Model; MEME/MAST, Multiple Em for Motif Elicitation/Motif Alignment and Search Tool; PtdIns, phosphatidylinositol; YPD, yeast extract, peptone, dextrose; 5-FOA, 5-fluoroorotic acid; 5-FAA, 5-fluoroanthranilic acid.

lysosomes. More recently discovered adaptor proteins, Gga's and epsins, are also involved in recruiting cargo in this transport route and are components of at least some AP-1–containing vesicles (reviewed by Robinson, 2004). These AP-1 or another class of clathrin-coated vesicles also mediate transport from the Golgi to the cell surface, either directly from the Golgi or to an endosomal intermediate (Fölsch *et al.*, 2001; Harsay and Schekman, 2002; Gall *et al.*, 2002; Ang *et al.*, 2004). However, clathrin does not appear to be involved in the major exocytic routes from the Golgi, so these pathways may rely on a mechanism of vesicle formation not involving coat proteins, or on yet-unidentified coat complexes. Possible coat proteins, FAPPs (four-phosphate adaptor proteins), that regulate exocytic transport from the TGN have been identified in mammalian cells (Godi *et al.*, 2004; Vieira *et al.*, 2005). The FAPP proteins bind to both Arf and PtdIns(4)P at the TGN and play a role specifically in non–clathrin-coated vesicle formation. One explanation for why coat proteins mediating cargo transport to the cell surface have been difficult to identify may be that there could be multiple, perhaps partially redundant, coat complexes with unique cargo specificities. A coat complex involved in transporting only a few cargoes from the Golgi to the plasma membrane in yeast and other fungi is the Chs5/6, or exomer, complex (Sanchatjate and Schekman, 2006; Trautwein *et al.*, 2006; Wang *et al.*, 2006).

The release of some types of vesicles, including clathrin-coated vesicles, from donor membranes involves dynamin GTPases (Damke *et al.*, 1994; Hinshaw, 2000) as well as various BAR domain proteins that directly modify membrane curvature (Peter *et al.*, 2004; Ren *et al.*, 2006). Actin and its regulators also play important roles in vesicle formation, both at the plasma membrane and the TGN (Engqvist-Goldstein and Drubin, 2003; Carreno *et al.*, 2004; Cao *et al.*, 2005; Egea *et al.*, 2006; Kessels *et al.*, 2006). Other regulators of vesicle fission, unique for TGN-to-plasma membrane transport in some cell types, are protein kinase D (PKD; Liljedahl *et al.*, 2001; Yeaman *et al.*, 2004) and CtBP/BARS (Weigert *et al.*, 1999). An effector of PKD is a PtdIns 4-kinase (Hausser *et al.*, 2005), the activity of which is critical for transport from the Golgi to the plasma membrane in both yeast and mammalian cells (Hama *et al.*, 1999; Walch-Solimena and Novick, 1999; Bruns *et al.*, 2002; Godi *et al.*, 2004). CtBP/BARS and PKD function only in the transport of cargo that have basolateral sorting signals (when expressed in either polarized or nonpolarized cells) and not in the transport of apical cargo (Yeaman *et al.*, 2004; Bonazzi *et al.*, 2005). Clearly, although some of the participants in exocytic transport from the TGN are known, other components are yet to be identified.

The genetic screens in yeast that identified many of the components of the exocytic machinery generally relied on a strong secretory block and temperature-conditional lethality. Such screens usually identified essential genes required for the transport of all (or most) cargo and likely missed genes that are required in only one of multiple routes from the Golgi to the cell surface. We therefore conducted a screen for new secretory mutants by using a mutant strain background that has a block in one of two known exocytic transport routes, so that a remaining route becomes essential. Using this strategy, we have identified a novel conserved protein that has a function in exocytic transport from the Golgi.

MATERIALS AND METHODS

Reagents and Growth of Yeast Strains

Minimal medium for growing plasmid-carrying yeast strains was CSM (complete synthetic medium) lacking a nutrient for plasmid selection, with amino acid mixes from Q-Biogene (Carlsbad, CA). All other growth media components were from Difco (Detroit, MI), and were prepared following recipes described by Sherman (2002). Rich medium was YPD (yeast extract, peptone, dextrose). All media contained 2% glucose unless otherwise stated. Although our *vps1*Δ and *vps1*Δ *apl2*Δ strains grew only slightly slower than wild-type cells at 37°C, the *vps1*Δ mutant has been reported to be temperature-sensitive in some strain backgrounds (Rothman *et al.*, 1990), so all cultures were maintained at 24°C unless otherwise noted. Culture growth was monitored by measuring OD_{600} in a Genesys 5 spectrophotometer (Spectronic Instruments, Westbury, NY).

PCR for cloning genes or for generating gene deletion fragments was performed using *Pfu* DNA polymerase (Stratagene, La Jolla, CA). All other DNA manipulating enzymes were from New England Biolabs (Beverly, MA). Other reagents were from Sigma-Aldrich (St. Louis, MO) unless otherwise stated.

Strains and Plasmids

Yeast Strains. The yeast strains used in this study are listed in Table 1. The strain 4513-216 is derived from strains described by Koshland *et al.* (1985); all other strains are derived primarily from S288C (Mortimer and Johnston, 1986). Crosses and tetrad analysis to generate yeast strains were performed as described by Sherman (2002). Yeast transformations for introducing plasmids or PCR products were by the lithium acetate method (Schiestl and Gietz, 1989). EHY767 was derived from eight sequential crosses of strains having EHY47, EHY362, 4513-216, and GPY1783-10A (Yeung *et al.*, 1999) backgrounds. EHY769 was generated from EHY441 by integrating a PCR product containing *apl2*Δ*::KAN* (generated using primers EH130, EH131; see below) from EUROSCARF strain Y14985 (Brachmann *et al.*, 1998). To disrupt *AVL9* in our *sec6-4* strain background, a PCR product containing *avl9*Δ*::KAN* from EUROSCARF strain Y12725 (generated using primers EH162, EH163) was integrated into EHY188 (Harsay and Schekman, 2002) to generate EHY883. Proper targeting of PCR products was confirmed by PCR analysis. The construction or origin of all other strains is described in Table 1.

Plasmids. Plasmid pEH134 was generated by ligating a PvuII-NotI fragment from pCKR18A containing *VPS1* (Rothman *et al.*, 1990) into the NotI and SmaI sites of a pRS316 vector (CEN, *URA3*; Sikorski and Hieter, 1989) that also contained *ADE3*. Plasmid pEH305 is a CEN plasmid containing the *TRP1* auxotrophic marker and the *APL2* gene and was constructed as follows: The *APL2* gene was generated by PCR from an S288C background using primers EH130, EH131, and the resulting PCR product was cloned into pCR-BluntII-TOPO using the Zero-Blunt TOPO kit (Invitrogen, Carlsbad, CA) to generate pEH301. A BamHI/NotI fragment containing the *APL2* gene from pEH301 was cloned into the BamHI/NotI sites of pRS314 (CEN, *TRP1*; Sikorski and Hieter, 1989) to generate pEH305. Plasmid pEH331 was constructed similarly and contains *APL2* in pRS316. Plasmid pEH414 contains a wild-type allele of *AVL9* and was constructed as follows: The *AVL9* gene was generated by PCR from an S288C background using primers EH164, EH165, and the resulting PCR product was cloned into pCR-BluntII-TOPO to generate pEH413. A BamHI/NotI fragment containing the *AVL9* gene from pEH413 was cloned into the BamHI/NotI sites of pRS313 (CEN, *HIS3*; Sikorski and Hieter, 1989) to generate pEH414. Plasmid pEH418 contains *AVL9* under the control of the *GAL1* promoter and was constructed as follows: The *AVL9* gene was generated by PCR using primers EH203 and EH165 and cloned into pCR-BluntII-TOPO to generate pEH416, from which a NotI/BamHI fragment was cloned into the NotI/BamHI sites of pHL012 (a CEN plasmid containing the *URA3* auxotrophic marker and the *GAL1* promoter, described by Liu *et al.*, 1992). The *AVL9* gene was completely sequenced from both directions to confirm a wild-type copy. Plasmid pEH419 was generated from pEH331 by swapping the *URA3* gene for *HIS3* using the pUH marker swapper plasmid (Cross, 1997) to generate a CEN *HIS3* plasmid containing the *APL2* gene. Plasmid pEH422 contains *AVL9* with its native promoter and was constructed from pEH413 and pRS316 using the strategy described for pEH414.

Primers. The primers mentioned above for strain and plasmid construction are as follows: EH130: TAACGCTTTACAAACAGAGCATA, EH131: TGAGAAATATTTAGATGGTGAAAGGGA, EH162: TGATGCTTGTCCGTCGGGT, EH163: CTTGTGGAGGTCACCCCAGTT, EH164: GCCTAGCAAAAATAGCCGCTG, EH165: TCTATTCCATTTTTGGAAAGCCCC, EH203: CCTCGCTGCAACCTTGTTGTCA.

Synthetic Lethal Screen

We used a colony sectoring scheme based on the color of *ade2 ade3* mutants to identify synthetic lethal mutants, similar to the approach described previously (Koshland *et al.*, 1985; Bender and Pringle, 1991). Overnight cultures of EHY771 or EHY1172 were grown to stationery-phase (to minimize budded cells) in CSM, −Ura medium, and mutagenized with ethyl methanesulfonate (EMS; according to Guthrie and Fink, 1991) to a 20–95% survival rate, in several screens. Cells were plated on YPD to obtain ~100 colonies per plate, and nonsectoring colonies were tested for lethality on 5-fluoroorotic acid plates (5-FOA) to test inability to lose a *URA-VPS1* or *URA-APL2* plasmid

Table 1. *S. cerevisiae* strains used in this study

Strain	Relevant genotype[a]	Source
4513-216	*MAT***a** *ade2-101 ade3 can1 leu2-3,112 ura3-52 his3-Δ200 sap3*	Bik Tye, Cornell University
GPY1783-10A	*MATα apl2Δ2::TRP1 his3-Δ200 leu2-3,112 trp1-Δ901 ura3-52 suc2-Δ9*	Yeung *et al.* (1999)
DBY1829	*MATα his3-Δ200 leu2-3,112 lys2-801 trp1-1 ura3-52*	T. Huffaker, Cornell University
CUY29	*MAT***a** *his3-Δ200 leu2-3,112 lys2-801 ura3-52* Gal^+	T. Huffaker, Cornell University
NY17	*MAT***a** *sec6-4 ura3-52*	Salminen and Novick (1987)
Y12725	*MATα his3-Δ1 leu2-Δ0 lys2-Δ0 ura3-Δ0 avl9Δ::kanMX4*	EUROSCARF BY4742 deriv.
Y14985	*MATα his3-Δ1 leu2-Δ0 lys2-Δ0 ura3-Δ0 apl2Δ::kanMX4*	EUROSCARF BY4742 deriv.
YMR3732-2B	*MATα rho3-1::TRP1 his3-Δ200 leu2-Δ1 lys2-801 ura3-52 trp1-Δ63 ade2-101*	Imai *et al.* (1996)
MBY004	*MAT***a** *gga1Δ::HIS5spL gga2ΔTRP1 ura3-52 leu2-3,112 his3-Δ200 trp1-Δ901 lys2-801 suc2-Δ9*	Black and Pelham (2000)
EHY46	*MATα leu2-3,112 lys2-801 trp1-1 ura3-52*	NY17 × DBY1829
EHY47	*MAT***a** *his3-Δ200 leu2-3,112 trp1-1 ura3-52*	NY17 × DBY1829
EHY225	*MATα sec6-4 vps1::LEU2 TPI::SUC2::HIS3 his3-Δ200 leu2-3,112 lys2-801 trp1-1 ura3-5*	Harsay and Schekman (2002)
EHY226	*MAT***a** *sec6-4 TPI::SUC2::URA3 his3-Δ200 leu2-3,112 trp1-1 ura3-52*	Harsay and Schekman (2002)
EHY239	*MAT***a** *TPI::SUC2::TRP1 his3-Δ200 leu2-3,112 trp1-1 ura3-52*	Harsay and Schekman (2002)
EHY361	*MAT***a** *vps1Δ::LEU2 his3-Δ200 leu2-3,112 trp1-1 ura3-52*	EHY47, integ. pCKR2
EHY362	*MATα vps1Δ::LEU2 leu2-3,112 lys2-801 trp1-1 ura3-52*	EHY46, integ. pCKR2
EHY441	*MAT***a** *vps1Δ::LEU2 ade2-101 ade3 lys2-801 leu2-3,112*	4513-216 × EHY362
EHY629	*MATα sec6-4 apl2Δ::TRP1 his3-Δ200 leu2-3,112 trp1-1 ura3-52 TPI::SUC2::URA3*	EHY226 × GPY1783-10A
EHY644	*MAT***a** *vps1Δ::LEU2 apl2Δ::TRP1 trp1 leu2-3,112 ura3-52 his3Δ*	GPY1783-10A × EHY661
EHY662	*MAT***a** *sec6-4 gga1Δ::HIS5spL gga2Δ::TRP1 his3-Δ200 leu2-3,112 lys2-801 trp1 ura3-52 TPI::SUC2::URA3*	EHY225 × MBY004
EHY767	*MATα vps1Δ::LEU2 apl2Δ::TRP1 ade2-101 ade3 leu2-3,112 trp1 ura3-52*	See *Materials and Methods*
EHY769	*MAT***a** *vps1Δ::LEU2 apl2Δ::KAN ade2-101 ade3 lys2-801 leu2-3,112 ura3-52*	EHY441 deriv. (see *Materials and Methods*)
EHY771	*MAT***a** *vps1Δ::LEU2 apl2Δ::KAN ade2-101 ade3 lys2-801 leu2-3,112 ura3-52* [*VPS1 ADE3 URA3*]	EHY769, tx pEH134
EHY840	*MAT***a** *avl9-1 vps1Δ::LEU2 apl2Δ::KAN ade2-101 ade3 lys2-801 leu2-3,112 ura3-52 trp1* [*APL2 TRP1*]	EHY771deriv. × EHY767, tx pEH305
EHY883	*MATα sec6-4 avl9Δ::KAN TPI::SUC2::HIS3 his3-Δ200 leu2-3,112 lys2-801 trp1-1 ura3-52*	EHY188 deriv. (see *Materials and Methods*)
EHY971	*MAT***a** *avl9-1 vps1Δ::LEU2 apl2Δ::KAN ade2-101 ade3 lys2-801 leu2-3,112 ura3-52 trp1* [*APL2 URA3*]	EHY771 deriv. × EHY767, tx pEH331
EHY1165	*MAT***a** *vps1Δ::LEU2 apl2Δ::TRP1 trp1 leu2-3,112 ura3-52 his3Δ* [*VPS1 URA3*]	EHY644 with pCKR18A
EHY1166	*MAT***a** *vps1Δ::LEU2 apl2Δ::TRP1 trp1 leu2-3,112 ura3-52 his3Δ* [*APL2 URA3*]	EHY644 with pEH331
EHY1172	*MATα vps1Δ::LEU2 apl2Δ::KAN ade2-101 ade3 leu2-3,112 trp1 ura3-52* [*VPS1 ADE3 URA3*]	EHY771 × EHY767
EHY1185	*MAT***a** *avl9Δ::KAN vps1Δ::LEU2 apl2Δ::TRP1 lys2 leu2 ura3 his3* [*APL2 URA3*]	Y14985 × EHY1166
EHY1226	*MAT***a** *avl9Δ::KAN vps1Δ::LEU2 apl2Δ::TRP1 lys2 leu2 ura3 his3* [*APL2 HIS3*]	EHY1185, swap plasmid to pEH419
EHY1227	*MAT***a** *avl9Δ::KAN vps1Δ::LEU2 apl2Δ::TRP1 lys2 leu2 ura3 his3* [$GAL1^p$*::AVL9 URA3*]	EHY1226, swap plasmid to pEH418
EHY1228	*MAT***a** *avl9Δ::KAN vps1Δ::LEU2 apl2Δ::TRP1 lys2 leu2 ura3 his3* [*AVL9 URA3*]	EHY1226, swap plasmid to pEH422
EHY1230	*MAT***a** *rho3-1::TRP1 vps1Δ::LEU2 apl2Δ::TRP1 trp1 leu2-3,112 ura3-52 his3Δ* [*VPS1 URA3*]	YMR3732-2B × EHY1165
EHY1236	*MAT***a**/*α his3-Δ1 leu2Δ0 lys2Δ0 ura3Δ0 avl9Δ::kanMX4*	Y12725 × Y12725 pHO-URA3
EHY1252	*MAT***a** *his3-Δ200 leu2-3,112 lys2-801 ura3-52* Gal^+ [*URA3*]	CUY29, tx pRS316
EHY1253	*MAT***a** *his3-Δ200 leu2-3,112 lys2-801 ura3-52* Gal^+ [$GAL1^p$*::AVL9 URA3*]	CUY29, tx pEH418

[a] All *ade3* strains are phenotypically His^- and may also be *his3-Δ200*. Genes borne by plasmids are indicated by brackets.

(pEH134 or pEH308). Mutants that were unable to grow on 5-FOA were transformed with a *TRP1 APL2* or *TRP1 VPS1* plasmid (pEH305, pEH314) and again tested for ability to grow on 5-FOA. Mutants that grew on 5-FOA when transformed with either of these plasmids have mutations that are lethal in combination with the *vps1Δ apl2Δ* double mutation. Such mutants were back-crossed to confirm 2:2 segregation of the synthetic lethal phenotype. Of 17 complementation groups, most with only one mutant member, one mutant had a consistently strong phenotype in repeated back-crosses. The complementing wild-type gene for this mutant, *avl9-1* (AP-1 Vps1 lethal 9), was cloned.

Cloning AVL9

The *AVL9* gene was cloned from a YCp50-based genomic library (*CEN, URA3*) created from genomic DNA prepared from EHY529, which lacked *VPS1* (E.H., unpublished reagent). The library had the advantage that we did not isolate *VPS1*-containing plasmids (which would be suppressors). Strain EHY840 (*avl9-1 vps1Δ apl2Δ* with an *APL2-TRP1* plasmid) was transformed with the library and plated on −Ura plates. Colonies were scraped and plated onto 5-fluoroanthranilic acid (5-FAA) plates, which do not allow cells with a *TRP1* gene to grow (Toyn *et al.*, 2000). Transformants that could grow on 5-FAA were able to lose the *TRP1 APL2* plasmid; these colonies were next streaked onto 5-FOA plates to ensure that the cells cannot grow (and therefore require the *URA3* plasmid from the library for suppression). Suppressor plasmids were isolated and sequenced at the insert junctions to identify the genomic DNA fragment responsible for suppression. This strategy yielded three library clones with overlapping ~10-kb inserts from chromosome XII. The suppressing gene from this region was identified by transposon mutagenesis of the plasmids using the GPS-1 Genome Priming System Kit (New England Biolabs). After transposon mutagenesis, the suppressor plasmid was transformed into *Escherichia coli*, transformed colonies were pooled, and plasmid DNA was isolated to generate a library of mutagenized plasmids. This library was transformed into EHY840, and transformants were screened for

inability to grow on FAA by replica-plating. Three nonsuppressing clones were isolated, and all were found to contain a unique insertion in the gene YLR114c.

Linkage of YLR114c with *avl9-1* was tested to determine whether it is the corresponding wild-type gene or a low-multicopy suppressor, as follows: The YLR114c genomic region was subcloned into an integrating (YIp) *URA3* plasmid (pRS306; Sikorski and Hieter, 1989), cut, and integrated into its chromosomal locus in a *vps1::LEU2 apl2::KAN avl9-1* strain. This strain was crossed to an *AVL9* strain with the opposite *MAT* type and lacking the integrant but otherwise identical, sporulated and dissected for tetrad analysis. None of the progeny exhibited the synthetic lethal phenotype; therefore, the integration was linked with the *avl9-1* gene. To further confirm that YLR114c is essential in a *vps1*Δ *apl2*Δ background, a strain having a deletion of YLR114c was obtained from the EUROSCARF yeast deletion collection (Y12725) and crossed to a *vps1*Δ *apl2*Δ strain to confirm the synthetic lethal phenotype.

To determine the nature of the *avl9-1* mutation, DNA of the mutant allele was generated by PCR, and two separate PCR reaction products were sequenced from both ends.

Subcellular Fractionation

Nycodenz gradient fractionation to characterize secretory vesicles was performed as described previously (Harsay and Schekman, 2002) except that rather than using a triethanolamine-acetic acid buffer with sorbitol for cell lysis and the gradients, the buffer contained 50 mM 2-(*N*-morpholino)ethanesulfonic acid (MES), pH 6.5, with KOH, 0.8 M sorbitol, and 1 mM EDTA. This change did not alter the gradient profiles observed for *sec6-4* and other strains tested. Enzyme assays were performed as previously described (Harsay and Schekman, 2002). For assaying gradient fractions by Western blots, the blots were processed as described previously (Harsay and Schekman, 2002). Images were captured in a ChemiDoc XRS digital darkroom (Bio-Rad, Richmond, CA) and quantified using Quantity One software (Bio-Rad).

Assays for Secretory Defects

Growth Conditions. For examining the effects of depleting Avl9p, cultures were grown overnight to log-phase in CSM, −Ura, 2% galactose, 2% raffinose, and 0.3% glucose and shifted into medium containing 2% glucose for 20 h, with dilution to maintain log-phase growth. For examining the effects of overexpressing Avl9p, cells were grown in CSM, −Ura with 2% glucose to log phase, and then transferred to CSM, −Ura, 2% raffinose, and grown overnight to log-phase. Growth in raffinose medium allows more rapid expression from the *GAL1* promoter after the shift to galactose. Cells were diluted to OD_{600} 0.05 in CSM, −Ura, 2% galactose, and 2% raffinose and growth was monitored at 1-h intervals for up to 15 h.

Bgl2p Accumulation Assay. Cells from 10 ml of culture (grown to OD_{600} 0.3–0.7) were collected by centrifugation and resuspended in ice-cold 10 mM NaN_3, 10 mM KF. After 10 min on ice, cells were incubated in prespheroplasting buffer (0.1 M Tris-H_2SO_4, pH 9.4, 50 mM β-mercaptoethanol (βME), 10 mM NaN_3, 10 mM KF) for 15 min on ice, washed in 1.4 M sorbitol, 50 mM KPi, pH 7, and 10 mM NaN_3 and resuspended in the same buffer with 170 μg/ml Zymolyase 100T (United States Biological, Swampscott, MA) for 30 min at 30°C with occasional gentle agitation. Cells were collected by centrifugation at 5000 × *g* for 10 min, pellets were resuspended in 200 μl of Laemmli sample buffer and heated for 5 min at 95°C, and 5 μl of sample was resolved by SDS-PAGE (Laemmli, 1970). Bgl2p and PGK were detected by immunoblot as previously described (Harsay and Schekman, 2002) except detection was with a ChemiDoc XRS imager (Bio-Rad).

Pulse-Chase Analysis. Cultures were grown in CSM media as described above and then shifted into CSM, −Met, −Cys at a density of 4 OD/ml. After 15 min, [^{35}S] Easytag Express Protein Labeling Mix (~1200 Ci/mmol, 14.3 mCi/ml, from Perkin Elmer-Cetus, Norwalk, CT) was added at 50 μCi/OD_{600} cells. After a 5-min labeling period, cold amino acid mix (50 mM methionine, 10 mM cysteine, 4% yeast extract, 2% glucose) was added for the indicated chase periods. One OD_{600} unit per immunoprecipitation reaction was removed and added to ice-cold 5× energy poison buffer (100 mM NaN_3, 100 mM KF, 0.5 M KPi, pH 7.5). After 10 min on ice, cells were converted to spheroplasts by the addition of 3× spheroplast buffer (0.3 mg/ml Zymolyase 100T, 2.8 M sorbitol, 50 mM βME) and incubation for 20 min at 36°C. Spheroplasts were chilled and gently centrifuged at 4°C for 10 min, 5000 × *g*, and pellets ("internal fraction") were separated from supernatants ("external fraction," containing medium and cell wall material). Supernatants were centrifuged again at 14,000 × *g* for 5 min to ensure complete removal of cells, diluted to 1 ml per original OD_{600} unit with H_2O, and trichloroacetic acid–precipitated using sodium deoxycholate as a carrier (Rexach *et al.*, 1994). Bgl2p or CPY was immunoprecipitated according to published procedures (Stirling *et al.*, 1992) and subjected to SDS-PAGE on 10% gels, which were analyzed by phosphorimaging on a Cyclone phosphorimager (Perkin Elmer-Cetus).

Invertase Secretion Assay. Cultures were grown in CSM media as described above. Cells from 10 ml of culture were collected by centrifugation, resuspended in 5 ml YPD medium with 5% glucose, and incubated with shaking for 1 h. Cells were then washed in H_2O, shifted to YPD medium with 0.1% glucose, and incubated with shaking for 90 min to derepress secretory invertase expression. They were then collected by centrifugation, resuspended in ice-cold energy poison (10 mM NaN_3, 10 mM KF) for 10 min, and diluted to 10 ml with H_2O for washing and to measure OD_{600}. Cells were again centrifuged and resuspended in 1 ml 0.2 M NaOAc, pH 4.9. The samples were split in two, and half the cells were permeabilized by the addition of 12 μl 20% Triton X-100 and freeze-thaw. This generated a "total" (permeabilized) fraction and an "outside/wall" fraction from unpermeabilized cells (Bankaitis *et al.*, 1990), which were assayed for invertase activity essentially as described (Goldstein and Lampen, 1975). Cell samples for each reaction originated from 0.02 OD_{600} cells (~5–10 μl of permeabilized or whole cell sample per 150 μl reaction).

Electron Microscopy

Supplies and reagents for electron microscopy (EM) were obtained from EMS (Hatfield, PA). For examining the effects of depleting Avl9p, we grew cells in CSM, −Ura medium with 0.3% glucose, 2% galactose, and 2% raffinose to log phase and then shifted them to CSM, −Ura medium with 2% glucose for 15 h (to OD_{600} ~0.3). They were then grown for 5 h in YPD with 2% glucose to obtain optimal morphology by EM. Cells were concentrated by vacuum filtration on a 0.2-μm filter to 7.5 ml, and 2.5 ml fixative was added to a final concentration of 2% formaldehyde, 2% glutaraldehyde, in 40 mM potassium phosphate buffer, pH 6.7. Cells were fixed with gentle agitation for 10 min and then collected by centrifugation and resuspended in fixative for continued fixation with gentle agitation for 45 min. Cells were then washed in 40 mM potassium phosphate, pH 6.7, postfixed in 4% $KMnO_4$ (Mallinckrodt, St. Louis, MO), stained en bloc with 0.5% aqueous uranyl acetate overnight, and processed for thin-section EM essentially as described by Wright (2000). Dehydration was in a graded series of ethanol and embedding was into Spurr's resin. Thin sections were stained with lead citrate (Reynolds, 1963) and stabilized by applying a thin layer of carbon with a Baltec vacuum evaporator (Boeckeler Instruments, Tuscon, AZ). Images were acquired on Kodak 4489 or SO-163 film (Eastman-Kodak, Rochester, NY) using a JEOL 1200 EX transmission electron microscope (TEM; Peabody, MA) operated at 80 or 100 kV. Negatives were scanned and images were adjusted for brightness and contrast using Photoshop CS (Adobe, San Jose, CA).

Cells for examining the effects of the *avl9*Δ mutation in a *sec6-4* background were grown as described in the figure legend and prepared as above. For examining the effects of overexpressing Avl9p, cells were grown in CSM, −Ura with 2% glucose to log phase, then transferred to CSM, −Ura, 2% raffinose and grown for two doublings (~7 h). Cells were then shifted into CSM, −Ura, 2% raffinose, and 2% galactose, grown for 11 h (while maintaining the culture in log-phase), and prepared as above for thin-section EM.

Light Microscopy

For experiments examining the effects of Avl9p depletion, cultures were grown as above for EM. Fixative (2.5 ml) was added to 10 ml culture, for a final concentration of 4% formaldehyde, 40 mM phosphate buffer, pH 6.7. Cells were fixed for 1 h and then overnight in fresh fixative. We followed published procedures to stain cells with caclofluor (Chant and Pringle, 1995). To visualize polymerized actin, fixed cells were washed with PBS, pH 7.4, permeabilized in 0.1% Triton X-100 for 15 min, washed four times in PBS, and stained in 0.1 U/μl Alexafluor-568 phalloidin (Molecular Probes, Eugene, OR) for 2 h. Washed cells were mounted in Prolong Gold Antifade (Molecular Probes) and observed with a 100×/1.4 PlanApochormat lens on an Axioplan 2ie microscope equipped with a motorized stage (Carl Zeiss MicroImaging, Thornwood, NY). Images were captured with a charge-coupled device camera (Orca ER, Hamamatsu Photonics, Bridgewater, NJ) and Openlab imaging software (Openlab; Improvision, Lexington, MA). *Z*-series were acquired in 0.2-μm steps and assembled and deconvolved using Volocity 2.6 software (Improvision). 2D projections were exported as TIFF files and adjusted for brightness and contrast in Photoshop CS.

Sequence Analysis

We identified orthologues of yeast Avl9p by BLAST searches (Altschul *et al.*, 1997) of the nr protein database using the NCBI BLAST server with default parameters. We also searched for protein families distantly related to Avl9p by PSI-BLAST using as query the most conserved regions of Avl9 proteins and consensi of these regions (~200–250 residues). Members of potentially related protein families were then further analyzed by ClustalW multiple sequence alignments (Thompson *et al., 1994*) and by the MEME/MAST system (Multiple Em for Motif Elicitation/Motif Alignment and Search Tool; Bailey and Elkan, 1994; Bailey and Gribskov, 1998), available at the San Diego Supercomputing Center (http://meme.sdsc.edu/meme/intro.html). Regions identified as similar by MEME/MAST were then used in new PSI-BLAST and MAST searches to identify more potentially related proteins, and these were then added to new MEME/MAST analyses. This process was repeated to generate a collection of potentially related protein sequences from represen-

tatives of diverse phyla. Five Avl9 homology (AH) regions of roughly ~50–100 residues each were defined by multiple MEME/MAST analyses using varying parameters. The combined AH regions as well as combined uDENN, DENN, and dDENN regions (as identified in the SMART database, Letunic *et al.*, 2004) from DENN-domain–containing proteins were aligned with ClustalW using Lasergene 7 software (DNASTAR, Madison, WI). To optimize the alignments, we also generated separate alignments containing subsets of proteins using T-Coffee (Notredame *et al.*, 2000) and Muscle (Edgar, 2004) and combined these with ClustalW alignments using T-Coffee. The aligned sequences were imported into MacVector 9 software (Accelrys, San Diego, CA) for editing of gaps by eye. The Entrez accession numbers for the sequences included in the alignment are as follows: DENN domain proteins: NP_079174, XP_397549, NP_079177, AAH36655; Avl9 proteins: XP_624093, NP_498416, XP_638363, NP_055875, XP_327309, CAA61692, CAB16239, EAR89363; ANR1 proteins: XP_394349, AAH40291, XP_783119, AAC02577, XP_641200, EAR85516; ANR2 proteins: EAL24019, XP_785244, P36090, XP_322253; MesA proteins: XP_646288, CAA22879, XP_657872, EAR95260; ANR3/Fam45 proteins: XP_782995, AAH22271; XP_647590; XP_001120151.

Phylogenetic reconstruction of the evolutionary relationships between Avl9 and related proteins was performed using the Phylip 3.66 software package, obtained from the author (Felsenstein, 2006). An inferred phylogenetic tree was generated by testing different trees and parameters in Phylip's maximum likelihood program, PROML, using as input the alignment obtained above along with user-defined trees generated by parsimony and distance matrix methods. The maximum parsimony user tree was generated using the PROTPARS program from Phylip, and a distance matrix tree was generated using PROTDIST with FITCH from Phylip, with the following parameters: Henikoff/Tillier PMB model of amino acid substitutions (Veerassamy *et al.*, 2003), Γ distribution of substitution rates among positions with coefficient of variation 0.45 (shape parameter α 4.9), Fitch-Margoliash criterion, multiple randomized input orders, and the global rearrangement option. The same distance matrix tree was generated by using the above PROTDIST matrix with a weighed neighbor-joining method, Weighbor (Bruno *et al.*, 2000). Estimated branch lengths were supplied to the most likely tested tree using PROML with a discrete approximation to Γ distributed substitution rates (four rate categories, α 4.9, PMB model of amino acid change). For bootstrap analysis (Felsenstein, 1985), pseudoreplicates of the alignment were generated using SEQBOOT from Phylip, and bootstrap trees were generated using PROTPARS (1000 replicates) and PROTDIST with FITCH (100 replicates). Consensus trees and bootstrap values were obtained using CONSENSE, and the tree was drawn using DRAWGRAM (Phylip). To test possible long-branch artifacts, additional analyses were performed with the exclusion of the ANR3 family proteins as well as with different DENN domains.

Protein secondary structure predictions were performed with the SAM (Karplus *et al.*, 1998, 2003) and PSIPRED (Jones, 1999; McGuffin *et al.*, 2000) algorithms. These two methods produced very similar predictions, but where they differed, PROFSec was used as tie breaker (Rost and Sander, 2000). All three prediction methods are freely available on the Web.

RESULTS

A Synthetic Lethal Screening Strategy for Identifying New Exocytic Mutants

Defects in cargo transport in two exocytic pathways in yeast can be assayed by density-gradient fractionation analysis of the secretory vesicles that accumulate in *sec* mutants, such as *sec6-4*, that have a temperature-conditional block in vesicle fusion with the plasma membrane. (Wild-type yeast cells are not suitable for such analysis because they have few exocytic vesicles.) Such fractionation analysis has identified two post-Golgi vesicle species with different densities and unique cargo (Harsay and Bretscher, 1995). A lighter vesicle species transports surface proteins such as the cell wall protein Bgl2p and an abundant plasma membrane ATPase, Pma1p, whereas a dense population of vesicles transports invertase and other enzymes that are secreted into the periplasm or growth medium. Both vesicle species transport an exoglucanase, but these exoglucanases are encoded by different genes.

To identify new genes involved in the post-Golgi exocytic pathway, we screened for mutants that are lethal in combination with a partial secretory block. We conducted our initial synthetic lethal screen with a strain having a *vps1*Δ mutation, with the rationale that in a mutant lacking the *VPS1* gene (encoding a dynamin homolog thought to be involved in vesicle formation at the TGN; Rothman *et al.*, 1990; Bensen *et al.*, 2000), invertase was missorted from the pathway mediated by high-density secretory vesicles to a pathway mediated by light-density vesicles (Figure 1A; Harsay and Schekman, 2002). Therefore, the *vps1*Δ mutant appears blocked in at least one exocytic transport route, and mutations that block a remaining route should cause lethality. However, this synthetic lethal screen was unsuccessful in identifying novel secretory mutants. Most likely, there are multiple alternate routes to the plasma membrane rather than just two, so just one mutation in addition to *vps1*Δ will rarely result in a lethal secretory defect. Alternatively, the *vps1*Δ mutation does not completely block the transport process in which Vps1p functions. Furthermore, Vps1p has recently been shown to be involved in processes other than secretion (Hoepfner *et al.*, 2001; Peters *et al.*, 2004). Therefore, the screen was modified so that the screen strain background contained both *vps1*Δ and another mutation in a gene involved in late secretory transport.

Promising additions to the *vps1*Δ mutation were suggested by results indicating that clathrin plays a role in the invertase-transporting pathway (Gall *et al.*, 2002; Harsay and Schekman, 2002). The AP-1 and Gga cargo adaptors appear to function together in the sorting of some cargo molecules into one species of clathrin vesicles at the TGN, but there is some evidence that they may function in separate pathways as well (Doray *et al.*, 2002; Ha *et al.*, 2003). It is not clear whether AP-1 functions primarily at the TGN, early endosomes, or both, either in yeast or mammalian cells (Valdivia *et al.*, 2002; Robinson, 2004). To better define the requirements of clathrin-mediated invertase transport and potentially identify a second mutation for our synthetic lethal screen, we examined the effects of an AP-1 defect (by deleting *APL2*, a gene encoding β-adaptin, a large AP-1 subunit), and a Gga defect (by deleting the two Gga genes in yeast, *GGA1* and *GGA2*) on sorting of exocytic cargo into the two characterized exocytic pathways. In the *apl2*Δ *sec6-4* mutant, much of the invertase accumulated in an intermediate-density compartment (Figure 1B), possibly representing a donor compartment from which invertase-transporting dense vesicles normally bud (based on fractionation profiles of organelle markers; Harsay and Schekman, 2002). This phenotype resembled that found for a *vps27*Δ *sec6-4* mutant (Harsay and Schekman, 2002). Vps27p is the yeast homolog of Hrs, an endosomal protein required for cargo sorting into multivesicular bodies (maturing early endosomes; Bache *et al.*, 2003; Katzmann *et al.*, 2003). More recently, Hrs has also been shown to function in cargo recycling from early endosomes to the plasma membrane (Hanyaloglu *et al.*, 2005; Yan *et al.*, 2005). However, in contrast to our results with *vps27*Δ *sec6-4*, the a*pl2*Δ *sec6-4* mutant appeared defective in the generation of, or sorting into, both classes of vesicles. Cargo normally in either light or dense vesicles was mostly in intermediate density fractions with small peaks at the densities where light and dense vesicles appear for the *sec6-4* strain. This was the case for invertase and exoglucanase (Figure 1B) as well as Pma1p and Bgl2p (not shown). Therefore, the *apl2*Δ mutation may cause a general transport or sorting defect at the Golgi.

The difference between the fractionation results for the *apl2*Δ and *vps1*Δ mutants suggests that transport blocks in the two mutants occur at different compartments, most likely the Golgi and endosomes. We found that the *gga1*Δ *gga2*Δ mutant had only a mild effect on sorting invertase into dense vesicles (Figure 1C), so mutations in these genes are less likely to be useful in our screens for exocytic mutants. We therefore constructed a new screen strain having a deletion of both the *VPS1* and *APL2* genes. Details of a syn-

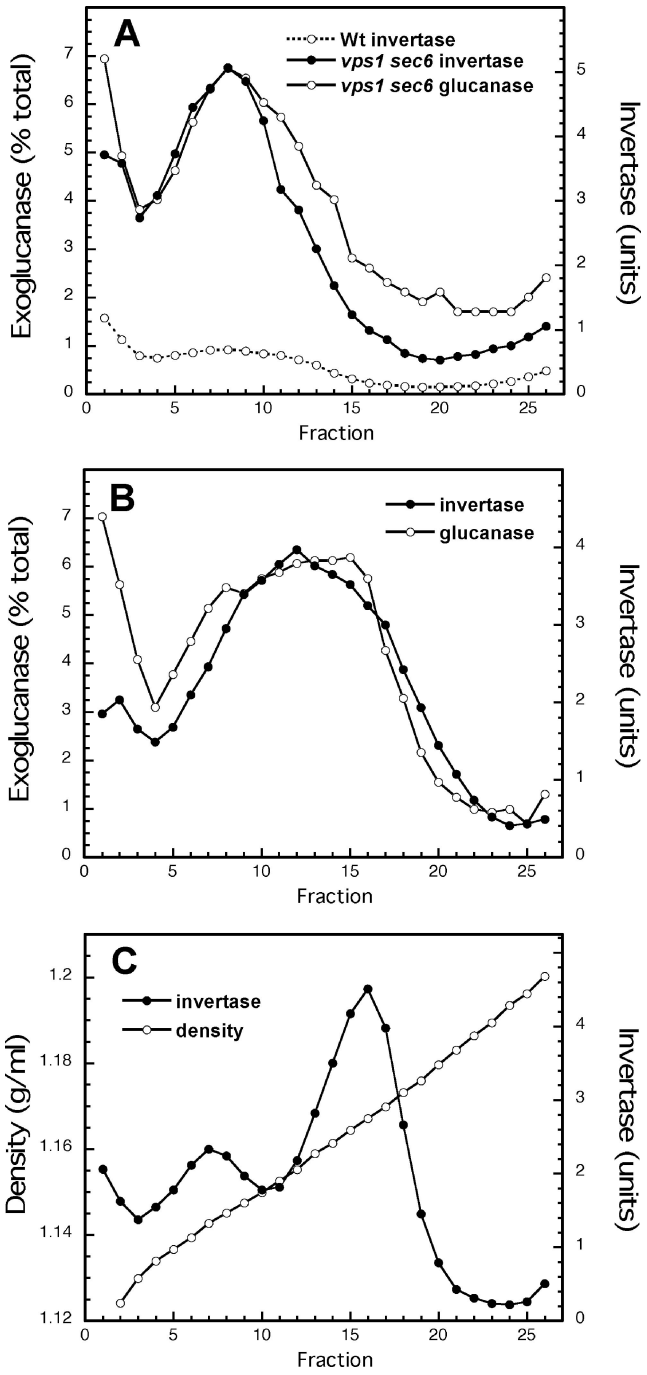

Figure 1. The *vps1*Δ and *apl2*Δ mutations have unique effects on invertase sorting into vesicles accumulated in a *sec6-4* mutant background. We used a Nycodenz density gradient fractionation assay in which secretory vesicles accumulated by a *sec6-4* mutant reproducibly peak in fraction 8 or 9 (light-density vesicles) or fractions 16–18 (high-density vesicles). (A) Nycodenz gradient fractionation of secretory vesicles accumulated in a *sec6-4 vps1*Δ mutant. All cargo is sorted into light-density vesicles, indicating a defect in the dense-vesicle transport pathway, as described previously (Harsay and Schekman, 2002). (B) The *apl2*Δ *sec6-4* mutant accumulates cargo primarily at a density intermediate between that of vesicles in the light-vesicle and dense-vesicle pathways. (C) The *gga1*Δ *gga2*Δ mutations have a relatively small effect on exocytic cargo transport in a *sec6-4* strain background. Invertase, which is a dense-vesicle cargo, is shown. The gradient density profile shown was highly reproducible for all gradients.

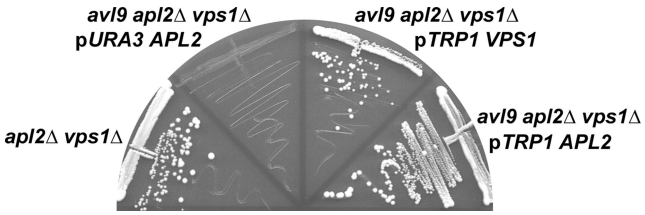

Figure 2. The *avl9-1* mutant is synthetically lethal in an *apl2*Δ *vps1*Δ strain background. The lethality of an *avl9-1 apl2*Δ *vps1*Δ strain carrying a *URA3-APL2* plasmid (or *URA3-VPS1* plasmid, not shown) on 5-FOA is rescued by introducing a *TRP1* plasmid containing either the *VPS1* or *APL2* genes.

thetic lethal screen using this strain background are described in *Materials and Methods*.

Our new screen was successful in yielding mutants with the desired synthetic phenotype: mutants that grow well in an otherwise wild-type background or when just *VPS1* or just *APL2* is absent, but which cannot survive in a *vps1*Δ *apl2*Δ background (Figure 2). We have cloned the corresponding wild-type copy for one of our mutants, *AVL9* , by a suppressor screen of the synthetic lethal phenotype (Supplementary Figure 1; see *Materials and Methods*). The gene was an uncharacterized ORF, YLR114c, coding for an 86-kDa protein. It is nonessential, and when deleted, the mutant has a synthetic lethal phenotype in the *apl2*Δ *vps1*Δ background, similar to what we found for the isolated mutant (in which a conserved Gly residue at position 52 is replaced by Asp).

Starting at amino acid residue 601, there are 20 nonsimilar amino acid differences between our *AVL9* sequences (from several strains, all S288C background) and the sequence reported in the SGD and Entrez databases (also S288C background). These changes, which include two Glu residues missing from the database sequence, are in a highly variable region of *AVL9* that is poorly conserved among *Saccharomyces* species and missing in most other species. We confirmed that this is a translated region by cloning and sequencing the *AVL9* cDNA from a cDNA library. The Avl9p homolog in *Drosophila melanogaster*, CG11178-PA, likewise has an unconserved C-terminal region (residues 606–708), and, like the region in yeast Avl9p, it is predicted to have disordered three-dimensional structure (when analyzed using the Disordered software; Ward *et al.*, 2004).

Depletion of Avl9p Results in a Secretory Phenotype and Accumulation of Golgi-like Structures

To observe the phenotype of the *avl9*Δ *vps1*Δ *apl2*Δ triple mutant, we attempted to generate a temperature-conditional allele of the *AVL9* gene. This was unsuccessful, so we instead created a plasmid construct containing *AVL9* under the control of the *GAL1* promoter, enabling expression of the gene in galactose-containing growth media and shut-off of expression in glucose-containing media. Triple-deletion strains carrying either this plasmid or a plasmid with *AVL9* under the control of its native promoter were grown to midlog phase in 2% galactose, 2% raffinose, and 0.3% glucose-containing minimal medium (medium for optimum growth; see below) and then shifted to 2% glucose-containing medium to shut off expression from the *GAL1* promoter. Growth was maintained for up to 20 h. We then assayed for secretion of secretory cargo in each of the two exocytic pathways: Bgl2p for the light-vesicle pathway and invertase for the dense-vesicle pathway.

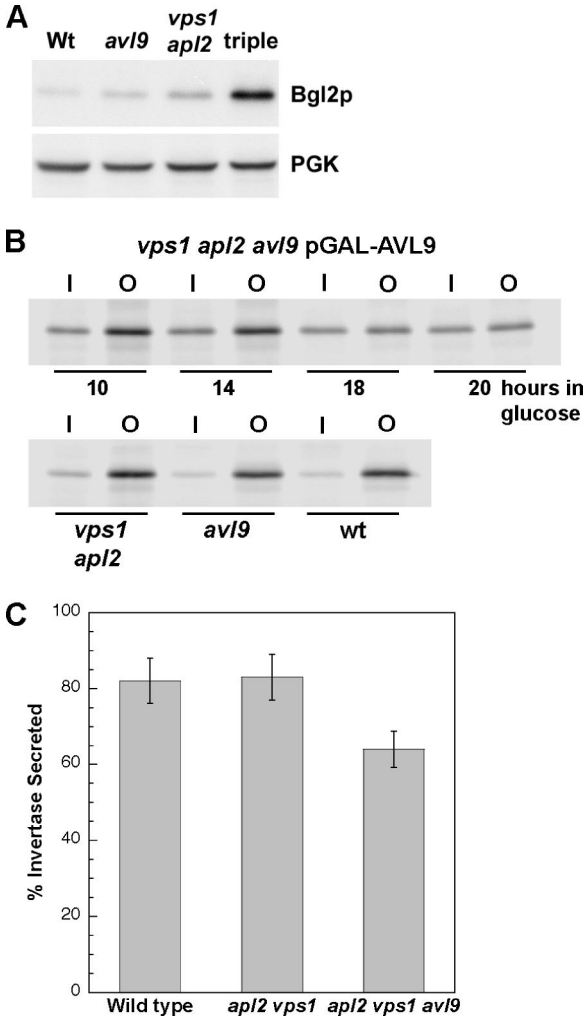

Figure 3. The *avl9*Δ *apl2*Δ *vps1*Δ mutant has defects in the exocytic pathway. (A) Western blot showing the accumulation of internal Bgl2p. The *avl9*Δ *apl2*Δ *vps1*Δ strain carrying a plasmid with *AVL9* under the control of the *GAL1* promoter was grown in medium containing 2% galactose, 0.3% glucose for optimal growth and then shifted to medium with 2% glucose for 20 h to deplete Avl9p. Bgl2p is primarily in the cell wall at steady state, so internal accumulation can be detected by removing the cell wall. PGK is a cytoplasmic protein used as loading control. (B) Metabolic labeling and pulse-chase analysis shows a kinetic defect in Bgl2p transport that becomes more pronounced with increased time in glucose to deplete Avl9p. Cells were pulse-labeled for 5 min, and chase was 60 min in each experiment. Cell walls were removed, and cells (I, inside) were separated from the cell wall and media fraction (O, outside). Bgl2p was immunoprecipitated and detected by SDS-PAGE and phosphorimaging. (C) Invertase secretion was assayed as described in *Materials and Methods*. External and total invertase levels were determined by a colorimetric enzyme assay to calculate percent secretion. The means of three experiments for each strain are shown. Error bars, SEM.

Bgl2p in wild-type cells is almost entirely in the cell wall, because very little internal Bgl2p is detected when the cell wall is gently removed by enzymatic digestion (Figure 3A). A similar result to wild type was observed for the *avl9*Δ mutant, and only slightly more than wild-type level of internal Bgl2p was observed for the *vps1*Δ *apl2*Δ double mutant. However, when galactose-dependent Avl9p was depleted in this mutant by growing cells in 2% glucose medium for 20 h, clear accumulation of Bgl2p was apparent. To assay the kinetics of Bgl2p secretion upon Avl9p depletion, we performed pulse-chase analysis of metabolically labeled Bgl2p (Figure 3B). A slight defect in Bgl2p secretion was observed after 10 h of Avl9p depletion in 2% glucose medium, with more severe defects noted after prolonged growth in 2% glucose. No obvious defect was detected for the *avl9*Δ or *vps1*Δ *apl2*Δ mutants. We also analyzed CPY secretion and processing in the same samples for *avl9*Δ and wild type and found no CPY transport defect (not shown).

An assay for invertase secretion likewise indicated a secretory defect upon Avl9p depletion in a *vps1*Δ *apl2*Δ background, with no defect observed for a *vps1*Δ *apl2*Δ strain (Figure 3C). Although the defect upon depleting Avl9p was not dramatic, it was similar to that obtained for some *sec* mutants, for example, *sec3*Δ (Grosshans *et al.*, 2006). We did not assay for Golgi processing of secretory proteins because *vps1*Δ strains have a glycosylation defect.

We prepared cells for thin-section EM to determine whether depleting Avl9p resulted in the accumulation or abnormal morphology of secretory organelles. Upon Avl9p depletion, the *apl2*Δ *vps1*Δ mutant accumulated abundant structures that resembled aberrant Golgi membranes seen in mutants with blocks in exit from the Golgi (Figure 4, A and B; Novick *et al.*, 1980; Walch-Solimena and Novick, 1999). Many cells also accumulated fenestrated membranes that resembled membranes seen in two temperature-sensitive mutants that block transport from the Golgi, *sec7* and *sec14*, after short shifts to restrictive temperature (Figure 4, C and D; Rambourg *et al.*, 1993, 1996). These results suggest that the secretory defects observed upon depletion of Avl9p are due to defective transport from the Golgi. This defect is observed only in the *vps1*Δ *apl2*Δ background with Avl9p depleted; an *avl9*Δ strain looks essentially wild type (Figure 4E). Very little abnormal membrane accumulation is observed in the *vps1*Δ *apl2*Δ double mutant (Figure 4F).

The avl9Δ Mutation Perturbs the Generation of Secretory Vesicles

To further examine the effect of the *avl9*Δ mutation on the late secretory pathway, we performed a subcellular fractionation assay (as in Figure 1) of a *sec6-4 avl9*Δ mutant to detect perturbations in the formation of late secretory vesicles. The result was similar to that found for the *apl2*Δ *sec6-4* mutant: secretory cargo normally in light or dense vesicles accumulated primarily in intermediate-density membranes (Figure 5). Therefore, like *apl2*Δ, the *avl9*Δ mutation appears to cause a defect in both secretory pathways, suggesting that Avl9p and Apl2p may function at the same compartment.

EM of the *avl9*Δ *sec6-4* mutant indicated the accumulation of Golgi-like structures and reduced secretory vesicle accumulation at the *sec6-4* restrictive temperature (Figure 6), so the accumulated intermediate-density membranes may represent vesicle donor compartments. The observed phenotype was heterogeneous, as some cells contained almost no vesicles, whereas others had abundant vesicles. Therefore, the intermediate density membranes may also include a third class of vesicles that is either an altered form of the normal light or dense vesicles, or is a third class of transport vesicles that is not sufficiently abundant to be detected in a strain with just a *sec6-4* mutation. Consistent with either possibility is our finding that these vesicles are slightly smaller than those observed in the *sec6-4* mutant (Figure 6, C and D).

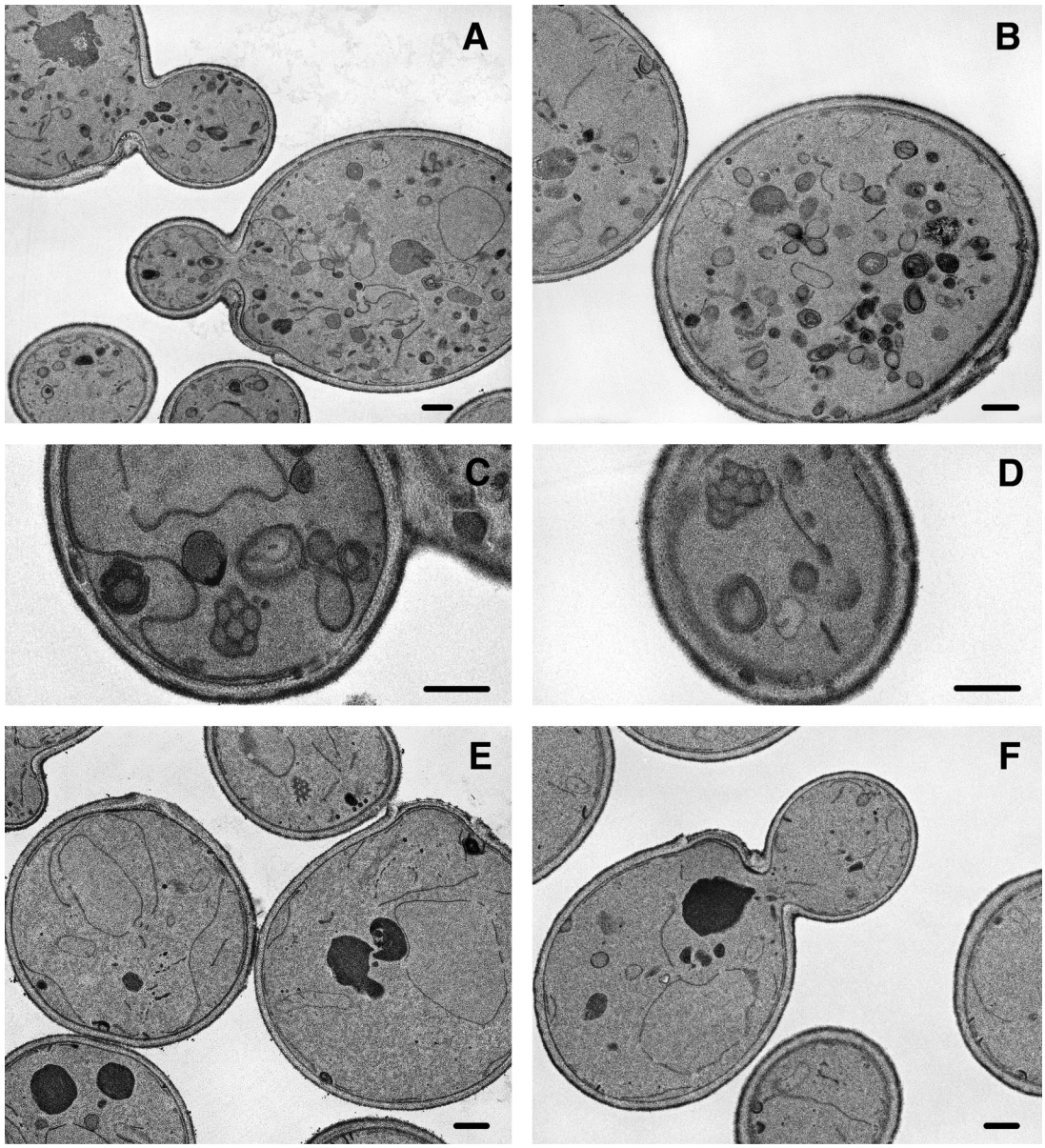

Figure 4. The *avl9*Δ *apl2*Δ *vps1*Δ mutant accumulates Golgi-like structures. (A–D) An *avl9*Δ *apl2*Δ *vps1*Δ strain carrying a plasmid with *AVL9* under the control of the *GAL1* promoter was grown as in Figure 3 to deplete Avl9p. Cells were prepared for thin-section EM after a 20-h shift to glucose. (E) An *avl9*Δ strain, prepared as above. (F) The *avl9*Δ *apl2*Δ *vps1*Δ mutant carrying a plasmid with *AVL9* under the control of its native promoter, prepared as above. Bars, 500 nm.

Depletion of Avl9p Results in Defects in Actin Polarization and Polarized Growth

In a genome-wide yeast two-hybrid screen of interacting yeast proteins, Avl9p was shown to bind only one protein, Rho3p (Ito *et al.*, 2001), a Ras-type small GTPase that regulates the actin cytoskeleton and is partially redundant with Rho4p (Matsui and Toh-E, 1992a,b). Rho3p and Cdc42p have some overlapping functions in the yeast exocytic pathway, but neither Rho protein appears to play a role in the VPS pathways to the vacuole (Adamo *et al.*, 2001). Cdc42 and other Rho proteins have functions in exocytic transport in mammalian cells as well (Kroschewski *et al.*, 1999; Müsch *et al.*, 2001). Although we were not able to confirm the interaction between Avl9p and Rho3p, we found that some *rho3* mutations, like *avl9* mutations, are synthetically lethal with *vps1*Δ *apl2*Δ, supporting the possibility that Avl9p may be involved in a Rho3p-mediated process. As shown in Supplementary Figure 2, the synthetic phenotype was observed at a normally permissive temperature for a temperature-sensitive allele, *rho3-1* (Imai *et al.*, 1996), as well as for the *rho3-V51* allele, which has defects in interacting with at least two effectors, Myo2p and Exo70 (not shown; Adamo *et al.*, 1999).

We determined whether actin distribution is perturbed in *avl9* mutants by staining cells with fluorescently labeled phalloidin to visualize polymerized actin (Figure 7, A–D). In wild-type cells, actin structures are highly polarized, with patches primarily in small- and medium-sized buds, and cables in mother cells (Adams and Pringle, 1984). This polarized actin distribution was largely lacking in the triple mutant after depleting Avl9p (Figure 7D). A large-scale analysis of yeast gene deletion mutants indicated that depolarized actin is not a general phenotype of sick mutants

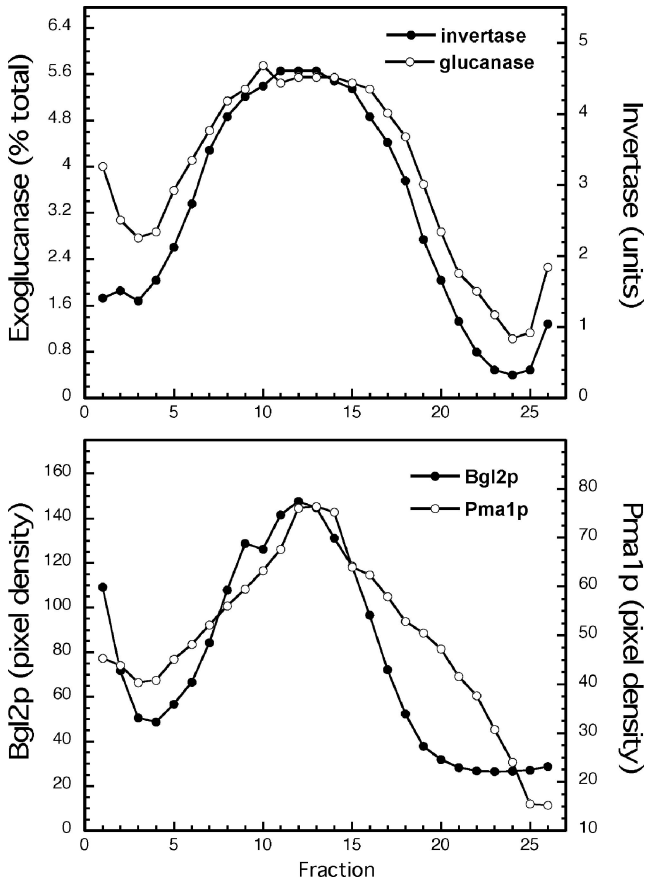

Figure 5. The *avl9*Δ *sec6-4* mutant accumulates cargo primarily in intermediate-density membranes, similar to what was observed for *apl2*Δ *sec6-4*. Density gradient fractionation was performed as for Figure 1.

(Karpova *et al.*, 1998), so this phenotype is likely to be related to Avl9p function. Two other mutants that perturb traffic in the TGN/endosomal system, *grd20* and *vps54*, likewise have depolarized actin distribution (Spelbrink and Nothwehr, 1999; Fiedler *et al.*, 2002). Because secretory traffic helps establish actin polarity (Zhang *et al.*, 2001; Wedlich-Soldner *et al.*, 2003; Aronov and Gerst, 2004), it is not clear whether this phenotype reflects primarily a defect in actin function or a defect in secretion or both. In either case, polarized secretion and growth is clearly perturbed, as indicated by often misshapen cells (Figure 7, D and G).

Secretory traffic travels along actin cables to the growing bud (Pruyne *et al.*, 1998; Schott *et al.*, 2002), and budding patterns also reflect whether secretory traffic is normally polarized. In haploid cells, new buds form adjacent to the previous bud at one pole of the cell (axial budding pattern) and leave a ring of chitin when they separate from the mother cell. In diploid cells budding occurs at either pole (bipolar budding pattern; Chant, 1999). Haploid *avl9*Δ *vps1*Δ *apl2*Δ mutant cells after Avl9p depletion frequently had a bipolar or random budding pattern (Figure 7, F and G), which was also occasionally noted in *vps1*Δ *apl2*Δ cells (Figure 7E), although most double-mutant cells showed a normal axial budding pattern. Haploid *avl9*Δ (single mutant) cells had a normal axial budding pattern (not shown) but in homozygous diploid *avl9*Δ cells, budding was random rather than bipolar (Figure 7I). The actin cytoskeleton was not noticeably perturbed in these cells (Figure 7C). A genome-wide screen of homozygous diploid yeast deletion mutants showed that several membrane traffic mutants, including a clathrin mutant, showed a strong random budding phenotype when diploid but had a normal budding pattern when haploid (Ni and Snyder, 2001), indicating that the bipolar budding pattern is especially sensitive to secretory defects.

Overexpression of Avl9p Is Toxic and Results in a Post-Golgi Secretory Defect

In the process of generating the strain for regulatable expression of *AVL9*, we found that maximum expression of *AVL9* from the strong *GAL1* promoter resulted in a severe growth defect, indicating that overexpression of the protein is toxic, in either *vps1*Δ *apl2*Δ cells (not shown) or wild-type cells (Figure 8). We compared growth in 2% galactose with 0, 0.1, 0.2, 0.3, or 0.4% glucose added to reduce *AVL9* expression and found that optimum growth was obtained when 0.3% glucose was added to galactose-containing medium.

We next examined the phenotype of cells overexpressing Avl9p by EM. Maximum expression from the *GAL1* promoter takes various lengths of time depending on strain background, but when cells are first grown in raffinose media, it generally takes ~2 h for expression to start, and at least 12 h for maximum expression (Schneider and Guarente, 1991). Therefore, cells were monitored for growth rate and fixed soon after growth had slowed down, to minimize possible indirect effects of Avl9p overexpression. Cells grown in galactose and minimal media have a dense cytoplasm with punctate structures when observed by EM (Wright, 2000), so the same strain containing an empty vector and grown under the same conditions was also prepared (Figure 9A). Cells overexpressing Avl9p showed clear accumulation of heterogeneous vesicles, suggesting the fragmentation of membrane compartments (Figure 9B). A few cells that overexpressed Avl9p also contained abnormal fenestrated membranes (Figure 9B). These structures were usually much larger, with more elongated fenestrations, than the fenestrated structures shown in Figure 4, C and D. Also, unlike the structures in Figure 4, C and D, they were connected with the nuclear envelope or endoplasmic reticulum (ER). Therefore, they are likely to be expanded ER membranes. Perhaps an organelle or organelles other than the ER is fragmented, which in turn could lead to eventual perturbations in ER morphology. The overexpression of Avl9p did not have any obvious effects on actin distribution, which was indistinguishable from wild type (not shown).

The phenotype observed by EM suggested that overexpression of Avl9p may produce a transport defect. Therefore, we assayed for a secretory defect in these cells. To establish optimal time points for these assays, log-phase growth rates were monitored at 1-h intervals for up to 15 h after shifting cells to galactose-containing medium, as described in *Materials and Methods* (Figure 10, A and B). Cells carrying an empty vector had no significant change in growth rate during this period, whereas the growth rate of cells overexpressing Avl9p slowed down by ~9 h of growth in galactose. The internal accumulation of Bgl2p was assayed 4, 8, and 12 h after growth in galactose (Figure 10C). There was a clear accumulation of internal Bgl2p by 8 and 12 h. Because this accumulation was observed at least 1 h before any slow-down in growth rate was detected, it was likely a direct effect of overexpressing Avl9p. Later time points were not assayed because by 14 h there was a significant decrease in newly synthesized Bgl2p (not shown), presumably because the cells adapted by decreasing the load

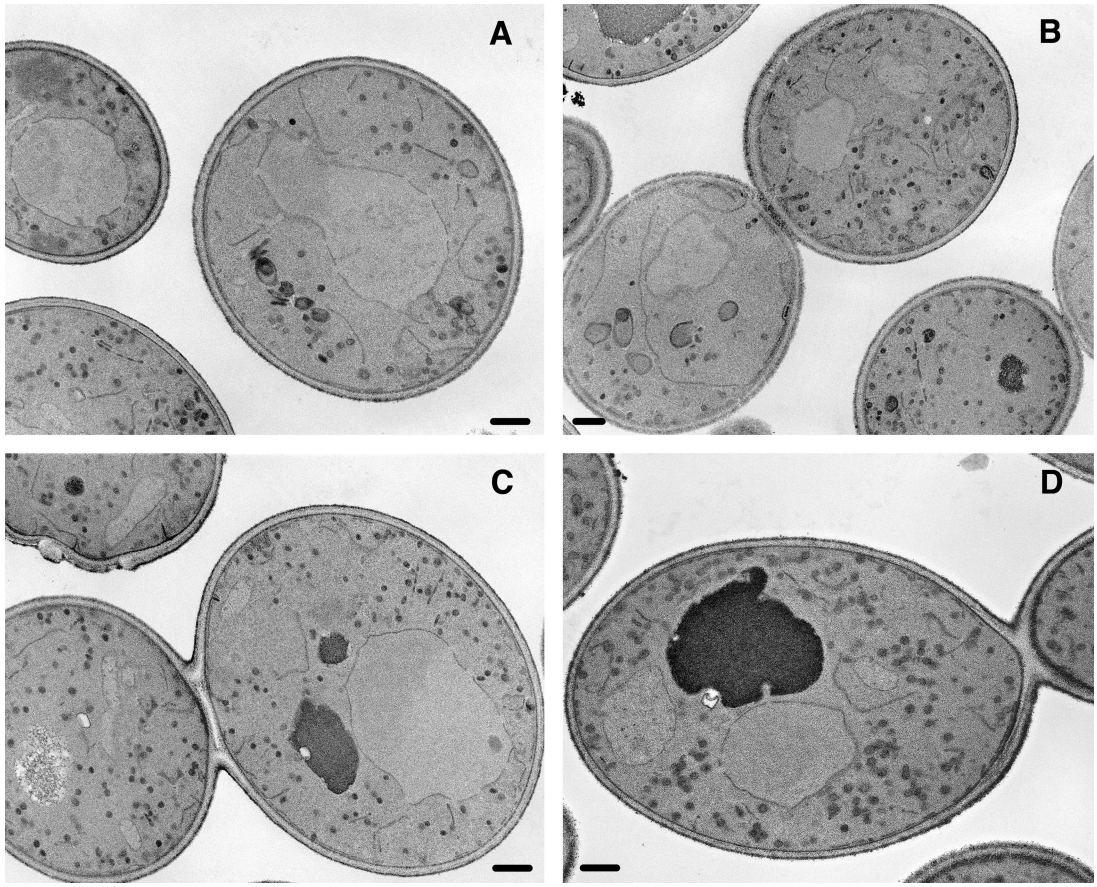

Figure 6. The *avl9*Δ mutation perturbs vesicle formation in a *sec6-4* strain background at restrictive temperature. Cells were grown to log-phase at 24°C and shifted to 36°C for 45 min before fixing for thin-section EM. (A–C) *avl9*Δ *sec6-4* mutant accumulates Golgi-like membranes and vesicles that are smaller than vesicles accumulated in a *sec6-4* mutant (D). Bars, 500 nm.

on the secretory pathway (Mizuta and Warner, 1994; Deloche *et al.*, 2004). The amount of newly synthesized Bgl2p was the same or decreased slightly from 2 to 12 h in galactose (Supplementary Figure 3). There was no defect in ER-to-Golgi transport of CPY in the same samples (Supplementary Figure 3). Even after 14 h in galactose, the rate of CPY transport to the vacuole was indistinguishable between control cells and cells overexpressing Avl9p (Figure 10C). Therefore, the transport defect appears to be specific for the late exocytic pathway.

Avl9p Is a Member of a Novel Protein Superfamily

AVL9 has orthologues in diverse eukaryotes, including metazoans and some primitive unicellular organisms, but it is absent in *Arabidopsis*. There is one gene per species, none of which have been previously characterized. The Avl9 proteins have two conserved regions of ~220–250 residues each, separated by an unconserved region of up to ~150 residues (Supplementary Figure 4A). The human, *Apis mellifera* (honey bee), *Caenorhabditis elegans*, and *S. cerevisiae* Avl9 proteins are on average 43% identical in the first conserved region and 37% identical in the second region (31 and 27% for the two regions in human and *S. cerevisiae* Avl9).

Our initial PSI-BLAST searches did not reveal clear paralogues of Avl9 proteins, and motif/domain databases did not indicate high-confidence homology to any previously characterized motifs. Therefore, in order to gain clues about Avl9p function, we performed PSI-BLAST searches using as queries the most conserved regions of Avl9 proteins from representative diverse species. We also performed MEME analyses and MAST searches, as detailed in *Materials and Methods*, to identify similar regions in potential homologues. This strategy was successful in identifying distantly related protein families that are difficult to align because conserved regions are separated by varying lengths of nonconserved regions. We identified four families of Avl9 paralogues, as well as a domain than is present in diverse proteins and is evolutionarily related to Avl9p and its paralogues. Five similar regions in these proteins were defined using MEME and MAST analyses (Figure 11). A criterion for defining these regions, termed AH (for Avl9 homology), was that they had to be readily identifiable in all or most proteins from diverse phyla for a given protein family. The AH regions have greatly varying distances of separation between, but generally not among, family members. AH3, followed by AH4, is the most conserved region between all Avl9 superfamily proteins, whereas AH5 is generally the most divergent region, although it is predicted to contain almost entirely alpha helices in all families. Although the AH regions were identified by the above methods and did not include predicted structure as a criterion, the regions appear to have similar secondary structures, as predicted by the SAM (Karplus *et al.*, 1998, 2003) and PSIPRED (Jones, 1999; McGuffin *et al.*, 2000) methods (Figure 11). We tried additional methods that work well for identifying distantly related proteins, including SAM, but these methods did not

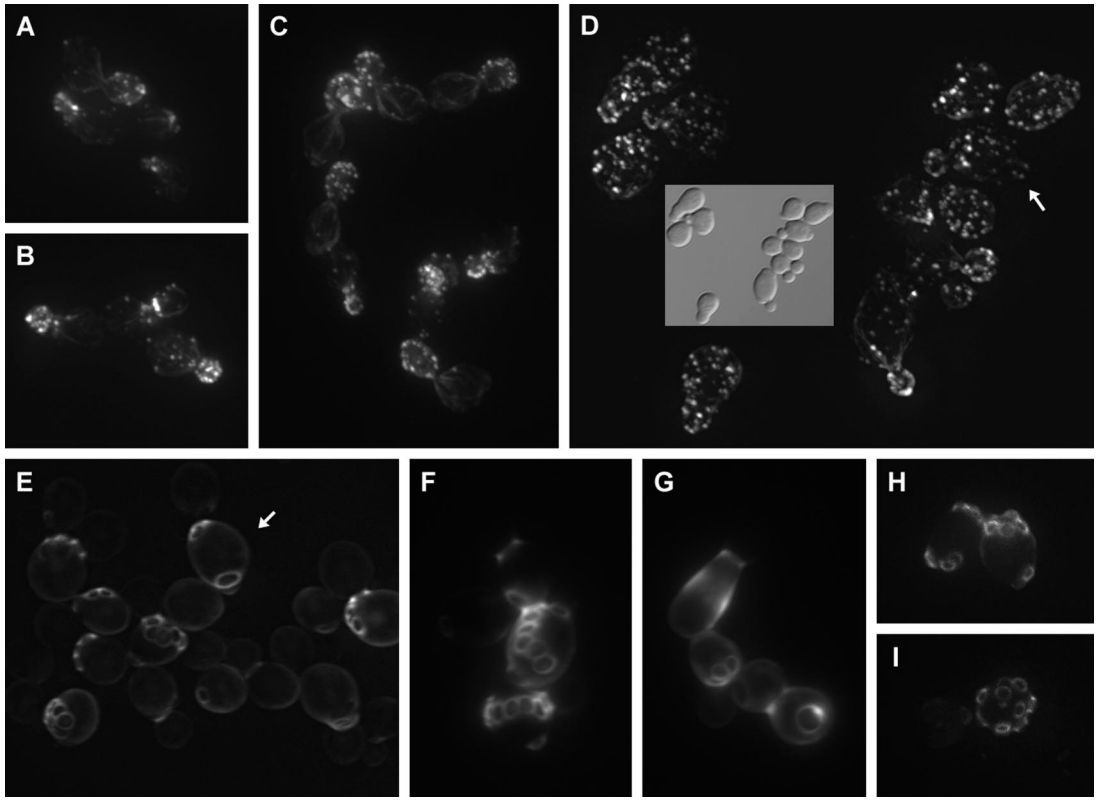

Figure 7. Polarized secretion is defective in *avl9* mutants. Cells were stained with Alexafluor-568 phalloidin to label polymerized actin (A–D) or with calcofluor to label chitin (E–I). (A) wt; (B) *apl2*Δ *vps1*Δ: (C) *avl9*Δ diploid; (D) *avl9*Δ *apl2*Δ *vps1*Δ after depleting Avl9p, as described in *Materials and Methods*; (E) *apl2 vps1*; (F, G) *avl9*Δ *apl2*Δ *vps1*Δ after depleting Avl9p; (H) wt diploid; (I) *avl9* diploid. All cells are at the same magnification except the DIC (differential interference contrast microscopy) inset in D. All cells are haploid unless otherwise noted. Arrows indicate abnormal budding pattern in haploid cells.

identify clearly related gene families in addition to those identified by the above procedure.

One of the Avl9-related protein families we identified is referred to as DUF1630 (domain of unknown function 1630, the "domain" being the entire protein) in the Pfam database (Bateman *et al.,* 2004), and here as ANR1 (for Avl nine–related family 1). ANR1 family members are found in diverse eukaryotes, including metazoans, fungi (but not *S. cerevisiae* or *S. pombe*), plants, and some primitive unicellular organisms (including *Tetrahymena*). There is usually one, sometimes two, genes per species, all uncharacterized. Analysis by both Pfam and SMART (Letunic *et al.,* 2006) indicates

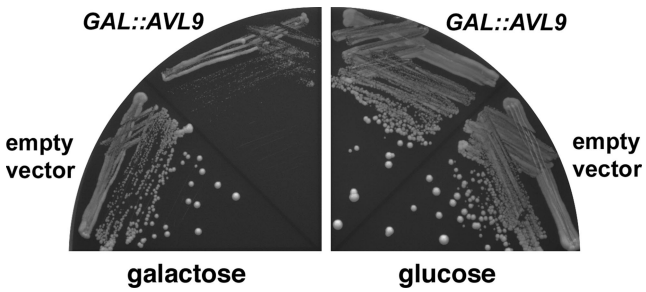

Figure 8. The overexpression of Avl9p is toxic. Strains EHY1252 (carrying a *URA3* CEN plasmid vector backbone) and EHY1253 (containing a *URA3* CEN plasmid with *GAL1*^{p}*::AVL9*) were streaked on CSM, −Ura plates with either 2% galactose or 2% glucose and grown for 3 days (galactose) or 2 days (glucose).

that the combined AH2, AH3, and AH4 regions in many ANR1 proteins have weak but significant similarity to the DENN domain (named after the DENN protein, Differentially Expressed in Normal vs. Neoplastic cells; Chow and Lee, 1996), and this similarity was also identified by the above PSI-BLAST and MEME/MAST analyses. The DENN protein is an isoform of MADD, a protein involved in MAPK signaling pathways (Schievella *et al.,* 1997). This protein is homologous to mammalian Rab3 GEF (guanine nucleotide exchange factor) and *C. elegans* AEX-3, which interacts with Rab3 in the regulation of synaptic vesicle exocytosis (Iwasaki *et al.,* 1997). The DENN domain is found in a wide range of other mammalian proteins, mostly with uncharacterized functions. It is usually flanked by two less-conserved regions, uDENN and dDENN (Levivier *et al.,* 2001). The uDENN regions have weak similarity to AH1 and the first ~10 residues of AH2, whereas dDENN has weak similarity to AH5. DENN-domain proteins are also found in fungi, plants, and primitive eukaryotes including amoebae and *Tetrahymena*, although in some of these cases there is no readily identifiable uDENN and/or dDENN region. *S. pombe* but not *S. cerevisiae* has a DENN-domain–containing protein.

The AH1-5 regions, always in consecutive order, are present in three other protein families: ANR2 (for Avl nine–related family 2), ANR3, and MesA families. The ANR2 family members are all uncharacterized proteins that are present in diverse eukaryotes. These include metazoans and yeasts, but not plants or primitive unicellular eukaryotes. The human protein is named KIAA1147 in Entrez. The

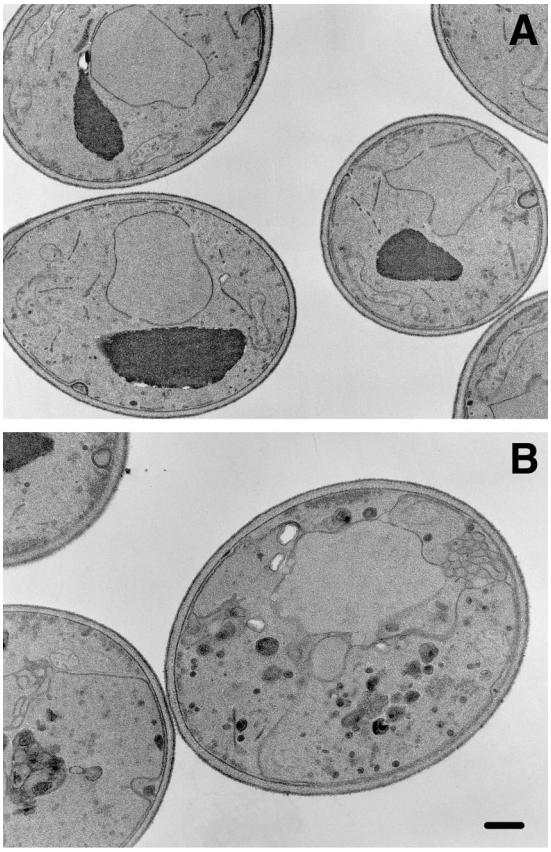

Figure 9. The overexpression of Avl9p results in perturbation of membrane organelles. The strains described in Figure 8 were grown as described in *Materials and Methods* and processed for thin-section EM soon after growth rate slowed down in galactose medium. (A) Wild-type cells grown under these conditions have a dense cytoplasm with small punctate structures. (B) Cells overexpressing Avl9p accumulate heterogeneous vesicles and expanded ER membranes. The images are at the same magnification. Bar, 500 nm.

ANR3 protein family, likewise uncharacterized, is referred to as Family 45 (Fam45) in Entrez. This family is found in vertebrates, sea urchin, honey bee (but not *Drosophila*), and *Dictyostelium*. The MesA family proteins are found primarily in fungi, with distant orthologues in primitive unicellular eukaryotes. MesA in *Aspergillus nidulans* was found in a screen for mutants that enhance morphogenesis defects caused by mutation of the actin nucleator formin (Pearson *et al.*, 2004). The MesA proteins are well conserved in filamentous fungi and likely perform a similar function, whereas the distant orthologues in nonfilamentous fungi such as *S. cerevisiae* and *S. pombe* do not have an obvious role in morphogenesis, and their functions are unknown (Pearson *et al.*, 2004). A yeast two-hybrid study suggests that the yeast MesA family member, Yor129cp, interacts with a component of the spindle pole body (Wysocka *et al.*, 2003).

To reconstruct the evolutionary relationships between the Avl9 family and related protein families, we generated alignments containing the AH1, 2, 3, and 4 regions as well as the uDENN and DENN and regions, as described in *Materials and Methods* (Supplementary Figure 4B). An identity matrix showing the percent identities between these regions is shown in Supplementary Figure 4C. For each protein family, four or more diverse species were included in order to provide data points that helped bridge the different families. An exception was uDENN/DENN. DENN domain proteins have many paralogues with complex phylogenies, so we included representative DENN domains that were among the least diverged from Avl9 superfamily proteins. A phylogenetic tree generated from the alignment is shown in Figure 12. Including the AH5 and dDENN regions in the alignment generated a similar tree, but these regions were excluded from the final tree analysis because they were difficult to align accurately. A likely rooting for the tree, based on distant homology to P-loop NTPases, is shown, but it is not clear which family is closest to the ancestral protein.

Different methods of generating trees, including maximum parsimony, in which a tree requiring the least number of mutations is generated, and distance methods, in which a tree is built based on a distance matrix generated from the alignment, produced trees with very similar topologies, indicating that the trees are likely accurate. Bootstrap analysis (Felsenstein, 1985) of maximum parsimony and distance matrix trees indicated good precision at most nodes (Figure 12). Bootstrapping is a statistical analysis of the robustness of a tree by the generation of pseudoreplicate samples of the alignment. This is done a large number of times and a tree is generated for each sample. The bootstrap value is the percent of time a given branch point occurs. Maximum likelihood analysis using the PROML software also supported the tree topology shown.

DISCUSSION

We used a triple-mutant synthetic lethality screen to identify components of the late secretory pathway transport machinery. This strategy resulted in the identification of a novel protein, Avl9p, that has a function in exocytic transport from the Golgi. The need for an elaborate screen to identify Avl9p as a component of a transport machinery reflects the complexity of the late secretory pathway. This complexity is due to numerous alternative transport routes, which was the basis for the design of our screen, but a probable further complexity is redundancy in transport machineries within a transport route. Therefore, future similar screening strategies may identify additional novel players in post-Golgi transport.

Avl9p orthologues are found in diverse species including humans, but none of these orthologues have been previously studied. Therefore, we used a combination of HMM-based similarity analysis and phylogenetic reconstruction to identify distant homologues in order to gain insights into Avl9p function. Our analysis revealed a novel superfamily that includes four protein families that are paralogous to Avl9 proteins, as well as an evolutionary relationship between this superfamily and an ancient domain, DENN, that is present in a large group of diverse proteins in most eukaryotic phyla. The presence of DENN domains, Avl9, and most Avl9 paralogues in both unikonts (amoebae, fungi, and metazoans) and bikonts (including plants, and protozoa such as *Tetrahymena*) indicates that these proteins were present very early in eukaryotic evolution, as the unikont/bikont bifurcation is believed to be the oldest evolutionary diversification of known eukaryotes (Stechmann and Cavalier-Smith, 2003). Therefore, Avl9p and its closest homologues likely have important roles in basic eukaryotic cell functions.

Although DENN-domain containing proteins are largely uncharacterized, they are the best-studied proteins with clear homology to Avl9p. Unlike the DENN-homology regions in Avl9 paralogues DENN is generally a domain within a much larger, multidomain mosaic protein, and the

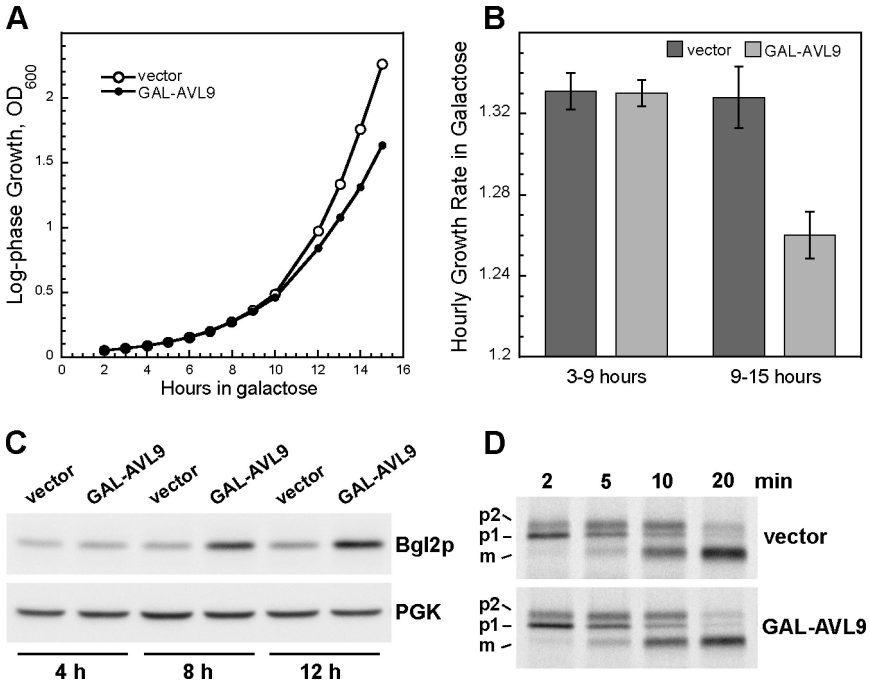

Figure 10. Overexpression of Avl9p results in a post-Golgi secretory defect. (A) The strains described in Figure 8 were grown as described in *Materials and Methods*, and growth after shift to galactose-containing medium was monitored. A slow-down in growth-rate was detectable by 9 h in galactose for cells with *GAL1p::AVL9*. (B) Comparison of the hourly growth rate (fold increase in OD_{600} after 1 h of growth) for cells containing a *URA3* CEN plasmid with *GAL1p::AVL9* or an empty *URA3* CEN vector. For 3–9 h, n = 6; for 9–15 h, n = 4. Error bars, SEM. (C) Internal Bgl2p was assayed at the indicated times after shift to galactose, as described for Figure 3. (D) Pulse-chase analysis of CPY transport after 14 h in galactose-containing medium, performed as described in *Materials and Methods*.

diversity of additional domains in these proteins indicates diverse functions. The additional domains can include, for example, RUN, GRAM, PLAT, PH, C2, WD40, LIM, and novel domains with unknown functions. Furthermore, the gene in which the domain was first identified, MADD/DENN/IG20 (Insulinoma-Glucagonoma 20), has at least four splice variants with diverse functions, which include regulation of apoptosis and cell proliferation (Mulherkar *et al.*, 2006). The MADD isoform interacts with tumor necrosis factor receptor to activate MAP kinase (Schievella *et al.*, 1997), and at least one isoform has a Rab3 GEF activity (Wada *et al.*, 1997). Another DENN-domain containing protein, ST5 (Suppression of Tumorigenicity 5) likewise has splice variants with different activities, at least some of which function in Ras signaling pathways and regulate the actin cytoskeleton (Hubbs *et al.*, 1999; Majidi *et al.*, 2000).

The possibility that some Avl9 orthologues may be involved in signaling pathways similar to those regulated by some DENN proteins is suggested by a large-scale two-hybrid screen of fly proteins that indicated an interaction between fly Avl9 and Traf3 (Giot *et al.*, 2003). Traf3 is a member of the TRAF family (tumor necrosis factor receptor–associated factors), the members of which are involved in a wide range of signaling pathways that regulate cell survival, proliferation, and differentiation (Lee and Lee, 2002). The same large-scale two-hybrid screen of fly proteins also indicated that Traf3 interacts with a Rho GAP, suggesting a signaling function that may involve actin regulation.

The closest Avl9p paralogue with any known function is MesA, first described for *A. nidulans* (Pearson *et al.*, 2004). The *mesA1* mutant allele in *A. nidulans* was found to cause defects in hyphal morphogenesis, and it exacerbated defects

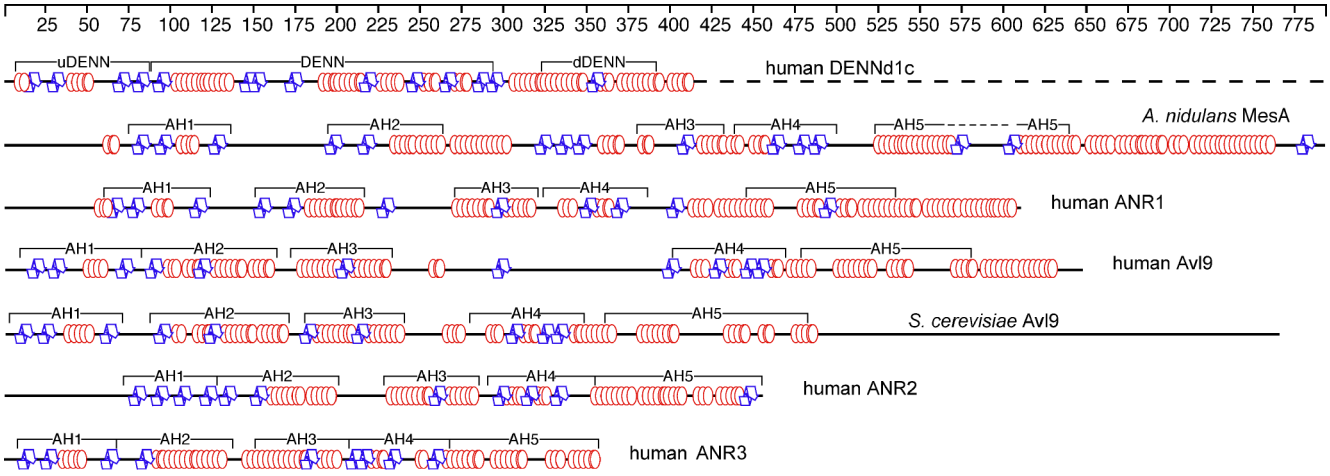

Figure 11. Conserved regions between Avl9 superfamily members, designated AH1-AH5, have similar secondary structure predictions. Predicted alpha helices are red and beta folds are blue. All proteins are drawn at the same scale, which is indicated in amino acid residues. Full-length proteins are shown. For DENNd1c, predicted structures are shown only for the uDENN, DENN, and dDENN regions. In some proteins, including MesA, AH5 is interrupted by an unconserved region.

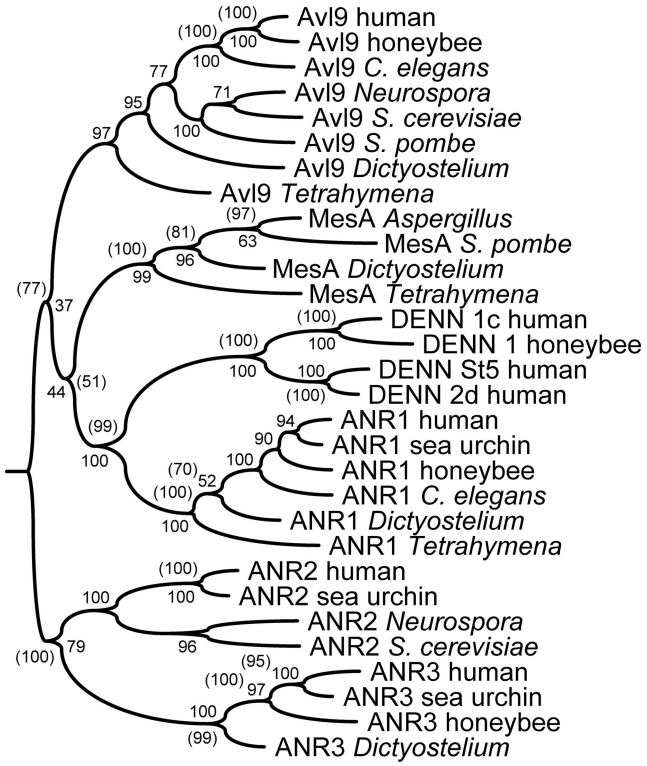

Figure 12. An inferred phylogenetic tree showing the relationships among Avl9 superfamily proteins and DENN domains, based on aligned AH1-4 and uDENN/DENN regions. Branch lengths were estimated by the maximum likelihood program PROML from the Phylip software package. Bootstrap values are indicated for both distance and parsimony (parenthesis) methods. Only one number is given for branching that differed between the two methods. The accession numbers for the sequences used are listed in *Materials and Methods*. The alignment used to produce the tree is shown in Supplementary Figure 4B.

in a formin mutant. Formins are nucleators of actin filaments (Pruyne *et al.*, 2002; Sagot *et al.*, 2002), and the MesA protein was shown to promote localized assembly of actin cables, perhaps indirectly by localizing formin to hyphal tips (Pearson *et al.*, 2004). The MesA and Avl9 proteins in various species are only ~25–30% identical in the combined AH1-4 regions, so the proteins likely have different functions. Nevertheless, the shared AH regions suggest that they may function by a similar mechanism or may interact with some of the same proteins.

We were not able to confirm the physical interaction between Rho3p and Avl9p that was suggested by a large-scale two-hybrid screen (Ito *et al.*, 2001). However, for all Avl9-related families, the SMART algorithm identified possible homologies to several motifs that are also found in GTPase regulators (for example, TBC and RhoGEF motifs). Although in each case these were poor matches (scoring worse than the default cutoff), they usually had the highest confidence scores of all matches and were found in at least some members of each family. Therefore, these similarities, our experimental results, and the homology to MesA and DENN together suggest the possibility that Avl9p may be involved in a Rho-mediated, actin-dependent transport process in the late secretory pathway.

Our EM and subcellular fractionation results indicated a role for Avl9p in generating secretory vesicles. In mammalian cells, actin is known to have functions in vesicle biogenesis at the Golgi (Carreno *et al.*, 2004; Cao *et al.*, 2005; Kessels *et al.*, 2006). A similar role for actin in generating vesicles at the yeast Golgi has not been clearly established, although it has long been known that actin mutations cause the accumulation of Golgi-like membranes and secretory cargo (Novick and Botstein, 1985). Karpova *et al.* (2000) showed that depolymerizing actin in yeast using latrunculin did not block secretion, but instead resulted in a defect in polarized vesicle transport and some vesicle accumulation. However, these studies did not address transport in all exocytic pathways, so it is possible that the generation of some classes of vesicles was blocked by latrunculin.

Although we propose that Avl9p has a function at the Golgi, the accumulation of Golgi-like structures does not necessarily indicate that Avl9p is directly involved in exit from the Golgi. A similar phenotype was observed by EM of a *trs120* mutant, which is defective in tethering vesicles in a recycling pathway from early endosomes to late Golgi (Cai *et al.*, 2005). Therefore, it is conceivable that Avl9p also, or primarily, plays a role in traffic from early endosomes. There is evidence for a role of actin and Rho proteins in transport from endosomes in mammalian cells (Sheff *et al.*, 2002; De Toledo *et al.*, 2003; Wherlock *et al.*, 2004).

One possible function of Avl9p in vesicle formation is a role in deforming membranes for vesicle fission. This is supported by our Avl9p overexpression experiments, which resulted in toxicity and the accumulation of heterogeneous vesicles. Alternatively or in addition, Avl9p may have a function in recruiting cargo. Interestingly, Avl9 superfamily proteins may contain regions with three-dimensional structural similarity to VHS/ENTH domains and HEAT repeats, as suggested by three-dimensional structure predictions made by the Rosetta algorithm (Simons *et al.*, 1999; Bonneau *et al.*, 2002), available at the Robetta server (Kim *et al.*, 2004; Chivian *et al.*, 2005). Similar predictions were made by the Tasser algorithm (Zhang and Skolnick, 2004). The Robetta predictions were ab initio rather than comparative modeling, because the fold recognition/threading algorithms used by the server (3D Jury; Ginalski *et al.*, 2003) did not make high-confidence matches between proteins with solved structures and any of the Avl9 superfamily proteins or DENN domains that we submitted for analysis. This suggests the possibility of novel folds and novel functions for a superfamily of largely uncharacterized, conserved eukaryotic proteins.

ACKNOWLEDGMENTS

We are grateful to the Texas A&M Microscopy and Imaging Center for allowing use of their TEM and to Paul de Figueiredo for hosting E.H. for a visit there. We also thank Yujie Li for preparing DNA for sequencing, Bill Dentler and David Moore for advice on microscopy, and Yasushi Matsui and Pat Brennwald for *rho* mutants. This work was supported by the Howard Hughes Medical Institute and National Institutes of Health Grant R01 GM26755 to R.S. E.H. was supported in part by Grant P20 RR15563-06 from the Centers of Biomedical Research Excellence Program of the National Center for Research Resources and funds from the State of Kansas.

REFERENCES

Adamo, J. E., Rossi, G., and Brennwald, P. (1999). The Rho GTPase Rho3 has a direct role in exocytosis that is distinct from its role in actin polarity. Mol. Biol. Cell *10*, 4121–4133.

Adamo, J. E., Moskow, J. J., Gladfelter, A. S., Viterbo, D., Lew, D. J., and Brennwald, P. J. (2001). Yeast Cdc42 functions at a late step in exocytosis, specifically during polarized growth of the emerging bud. J. Cell Biol. *155*, 581–592.

Adams, A.E.M., and Pringle, J. R. (1984). Relationship of actin and tubulin distribution to bud growth in wild-type and morphogenetic-mutant *Saccharomyces cerevisiae*. J. Cell Biol. *98*, 934–945.

Altschul, S. F., Madden, T. L., Schaffer, A. A., Zhang, J., Zhang, Z., Miller, W., and Lipman, D. J. (1997). Gapped BLAST and PSI-BLAST: a new generation of protein database search programs. Nucleic Acids Res. *25*, 3389–3402.

Ang, A. L., Taguchi, T., Francis, S., Folsch, H., Murrells, L. J., Pypaert, M., Warren, G., and Mellman, I. (2004). Recycling endosomes can serve as intermediates during transport from the Golgi to the plasma membrane of MDCK cells. J. Cell Biol. *167*, 531–543.

Aronov, S., and Gerst, J. E. (2004). Involvement of the late secretory pathway in actin regulation and mRNA transport in yeast. J. Biol. Chem. *279*, 36962–36971.

Bache, K. G., Brech, A., Mehlum, A., and Stenmark, H. (2003). Hrs regulates multivesicular body formation via ESCRT recruitment to endosomes. J. Cell Biol. *162*, 435–442.

Bailey, T. L., and Elkan, C. (1994). Fitting a mixture model by expectation maximization to discover motifs in biopolymers. In: Proceedings of the Second International Conference on Intelligent Systems for Molecular Biology, Menlo Park, CA: AAAI Press, 28–36.

Bailey, T. L., and Gribskov, M. (1998). Combining evidence using p-values: application to sequence homology searches. Bioinformatics *14*, 48–54.

Bankaitis, V. A., Aitken, J. R., Cleves, A. E., and Dowhan, W. (1990). An essential role for a phospholipid transfer protein in yeast Golgi function. Nature *347*, 561–562.

Bankaitis, V. A., Johnson, L. M., and Emr, S. D. (1986). Isolation of yeast mutants defective in protein targeting to the vacuole. Proc. Natl. Acad. Sci. USA *83*, 9075–9079.

Bateman, A. *et al.* (2004). The Pfam protein families database. Nucleic Acids Res. *32*, D138–D141.

Bender, A., and Pringle, J. R. (1991). Use of a screen for synthetic lethal and multicopy suppressee mutants to identify two new genes involved in morphogenesis in *Saccharomyces cerevisiae.* Mol. Cell. Biol. *11*, 1295–1305.

Bensen, E. S., Costaguta, G., and Payne, G. S. (2000). Synthetic genetic interactions with temperature-sensitive clathrin in *Saccharomyces cerevisiae*: roles for synaptojanin-like Inp53p and dynamin-related Vps1p in clathrin-dependent protein sorting at the trans-Golgi network. Genetics *154*, 83–97.

Bonazzi, M. *et al.* (2005). CtBP3/BARS drives membrane fission in dynamin-independent transport pathways. Nat. Cell Biol. *7*, 570–580.

Bonneau, R., Strauss, C. E., Rohl, C. A., Chivian, D., Bradley, P., Malmstrom, L., Robertson, T., and Baker, D. (2002). De novo prediction of three-dimensional structures for major protein families. J. Mol. Biol. *322*, 65–78.

Brachmann, C. B., Davies, A., Cost, G. J., Caputo, E., Li, J., Hieter, P., and Boeke, J. D. (1998). Designer deletion strains derived from *Saccharomyces cerevisiae* S288C: a useful set of strains and plasmids for PCR-mediated gene disruption and other applications. Yeast *14*, 115–132.

Bruno, W. J., Socci, N. D., and Halpern, A. L. (2000). Weighted neighbor joining: a likelihood-based approach to distance-based phylogeny reconstruction. Mol. Biol. Evol. *17*, 189–197.

Bruns, J. R., Ellis, M. A., Jeromin, A., and Weisz, O. A. (2002). Multiple roles for phosphatidylinositol 4-kinase in biosynthetic transport in polarized Madin-Darby canine kidney cells. J. Biol. Chem. *277*, 2012–2018.

Cai, H., Zhang, Y., Pypaert, M., Walker, L., and Ferro-Novick, S. (2005). Mutants in trs120 disrupt traffic from the early endosome to the late Golgi. J. Cell Biol. *171*, 823–833.

Cao, H., Weller, S., Orth, J. D., Chen, J., Huang, B., Chen, J. L., Stamnes, M., and McNiven, M. A. (2005). Actin and Arf1-dependent recruitment of a cortactin-dynamin complex to the Golgi regulates post-Golgi transport. Nat. Cell Biol. *7*, 483–492.

Carreno, S., Engqvist-Goldstein, A. E., Zhang, C. X., McDonald, K. L., and Drubin, D. G. (2004). Actin dynamics coupled to clathrin-coated vesicle formation at the trans-Golgi network. J. Cell Biol. *165*, 781–788.

Chant, J. (1999). Cell polarity in yeast. Annu. Rev. Cell Dev. Biol. *15*, 365–391.

Chen, C. Y., Ingram, M. F., Rosal, P. H., and Graham, T. R. (1999). Role for Drs2p, a P-type ATPase and potential aminophospholipid translocase, in yeast late Golgi function. J. Cell Biol. *147*, 1223–1236.

Chen, Y. G., Siddhanta, A., Austin, C. D., Hammond, S. M., Sung, T. C., Frohman, M. A., Morris, A. J., and Shields, D. (1997). Phospholipase D stimulates release of nascent secretory vesicles from the trans-Golgi network. J. Cell Biol. *138*, 495–504.

Chivian, D., Kim, D. E., Malmstrom, L., Schonbrun, J., Rohl, C. A., and Baker, D. (2005). Prediction of CASP6 structures using automated Robetta protocols. Proteins *61*(Suppl 7), 157–166.

Chow, V. T., and Lee, S. S. (1996). DENN, a novel human gene differentially expressed in normal and neoplastic cells. DNA Seq. *6*, 263–273.

Cross, F. R. (1997). 'Marker swap' plasmids: convenient tools for budding yeast molecular genetics. Yeast *13*, 647–653.

D'Souza-Schorey, C., and Chavrier, P. (2006). ARF proteins: roles in membrane traffic and beyond. Nat. Rev. Mol. Cell Biol. *7*, 347–358.

Damke, H., Baba, T., Warnock, D. E., and Schmid, S. L. (1994). Induction of mutant dynamin specifically blocks endocytic coated vesicle formation. J. Cell Biol. *127*, 915–934.

Deloche, O., de la Cruz, J., Kressler, D., Doere, M., and Linder, P. (2004). A membrane transport defect leads to a rapid attenuation of translation initiation in *Saccharomyces cerevisiae.* Mol. Cell *13*, 357–366.

De Toledo, M., Senic-Matuglia, F., Salamero, J., Uze, G., Comunale, F., Fort, P., and Blangy, A. (2003). The GTP/GDP cycling of Rho GTPase TCL is an essential regulator of the early endocytic pathway. Mol. Biol. Cell *14*, 4846–4856.

Dong, Y., Pruyne, D., and Bretscher, A. (2003). Formin-dependent actin assembly is regulated by distinct modes of Rho signaling in yeast. J. Cell Biol. *161*, 1081–1092.

Doray, B., Ghosh, P., Griffith, J., Geuze, H. J., and Kornfeld, S. (2002). Cooperation of GGAs and AP-1 in packaging MPRs at the trans-Golgi network. Science *297*, 1700–1703.

Edgar, R. C. (2004). MUSCLE: multiple sequence alignment with high accuracy and high throughput. Nucleic Acids Res. *32*, 1792–1797.

Egea, G., Lazaro-Dieguez, F., and Vilella, M. (2006). Actin dynamics at the Golgi complex in mammalian cells. Curr. Opin. Cell Biol. *18*, 168–178.

Engqvist-Goldstein, A. E., and Drubin, D. G. (2003). Actin assembly and endocytosis: from yeast to mammals. Annu. Rev. Cell Dev. Biol. *19*, 287–332.

Felsenstein, J. (1985). Confidence limits on phylogenies: an approach using the bootstrap. Evolution *39*, 783–791.

Felsenstein, J. (2006). PHYLIP (Phylogeny Inference Package) version 3.66. Distributed by the author. Department of Genome Sciences, University of Washington, Seattle.

Fiedler, T. A., Karpova, T. S., Fleig, U., Young, M. E., Cooper, J. A., and Hegemann, J. H. (2002). The vesicular transport protein Cgp1p/Vps54p/Tcs3p/Luv1p is required for the integrity of the actin cytoskeleton. Mol. Genet. Genom. *268*, 190–205.

Fölsch, H., Pypaert, M., Schu, P., and Mellman, I. (2001). Distribution and function of AP-1 clathrin adaptor complexes in polarized epithelial cells. J. Cell Biol. *152*, 595–606.

Gall, W., Geething, N., Hua, Z., Ingram, M., Liu, K., Chen, S., and Graham, T. (2002). Drs2p-dependent formation of exocytic clathrin-coated vesicles in vivo. Curr. Biol. *12*, 1623–1627.

Ghosh, P., and Kornfeld, S. (2004). The GGA proteins: key players in protein sorting at the trans-Golgi network. Eur. J. Cell Biol. *83*, 257–262.

Ginalski, K., Elofsson, A., Fischer, D., and Rychlewski, L. (2003). 3D-Jury: a simple approach to improve protein structure predictions. Bioinformatics *19*, 1015–1018.

Giot, L. *et al.* (2003). A protein interaction map of *Drosophila melanogaster.* Science *302*, 1727–1736.

Goldstein, A., and Lampen, J. O. (1975). b-D-Fructofuranoside fructohydrolase from yeast. Methods Enymol. *42*, 504–511.

Grosshans, B. L., Andreeva, A., Gangar, A., Niessen, S., Yates, J. R., 3rd, Brennwald, P., and Novick, P. (2006). The yeast lgl family member Sro7p is an effector of the secretory Rab GTPase Sec4p. J. Cell Biol. *172*, 55–66.

Guo, W., Sacher, M., Barrowman, J., Ferro-Novick, S., and Novick, P. (2000). Protein complexes in transport vesicle targeting. Trend Cell Biol. *10*, 251–255.

Guthrie, C., and Fink, G. R. (1991). Guide to Yeast Genetics and Molecular Biology, New York: Academic Press.

Ha, S. A., Torabinejad, J., DeWald, D. B., Wenk, M. R., Lucast, L., De Camilli, P., Newitt, R. A., Aebersold, R., and Nothwehr, S. F. (2003). The synaptojanin-like protein Inp53/Sjl3 functions with clathrin in a yeast TGN-to-endosome pathway distinct from the GGA protein-dependent pathway. Mol. Biol. Cell *14*, 1319–1333.

Hama, H., Schnieders, E. A., Thorner, J., Takemoto, J. Y., and DeWald, D. B. (1999). Direct involvement of phosphatidylinositol 4-phosphate in secretion in the yeast *Saccharomyces cerevisiae.* J. Biol. Chem. *274*, 34294–34300.

Hanyaloglu, A. C., McCullagh, E., and von Zastrow, M. (2005). Essential role of Hrs in a recycling mechanism mediating functional resensitization of cell signaling. EMBO J. *24*, 2265–2283.

Harsay, E., and Bretscher, A. (1995). Parallel secretory pathways to the cell surface in yeast. J. Cell Biol. *131*, 297–310.

Harsay, E., and Schekman, R. (2002). A subset of yeast vacuolar protein sorting mutants is blocked in one branch of the exocytic pathway. J. Cell Biol. *156*, 271–285.

Hartman, J. L., IV, Garvik, B., and Hartwell, L. (2001). Principles for the buffering of genetic variation. Science *291*, 1001–1004.

Hausser, A., Storz, P., Martens, S., Link, G., Toker, A., and Pfizenmaier, K. (2005). Protein kinase D regulates vesicular transport by phosphorylating and activating phosphatidylinositol-4 kinase IIIbeta at the Golgi complex. Nat. Cell Biol. *7*, 880–886.

Hinshaw, J. E. (2000). Dynamin and its role in membrane fission. Annu. Rev. Cell Dev. Biol. *16*, 483–519.

Hirschberg, K., Miller, C. M., Ellenberg, J., Presley, J. F., Siggia, E. D., Phair, R. D., and Lippincott-Schwartz, J. (1998). Kinetic analysis of secretory protein traffic and characterization of golgi to plasma membrane transport intermediates in living cells. J. Cell Biol. *143*, 1485–1503.

Hoepfner, D., van den Berg, M., Philippsen, P., Tabak, H. F., and Hettema, E. H. (2001). A role for Vps1p, actin, and the Myo2p motor in peroxisome abundance and inheritance in *Saccharomyces cerevisiae.* J. Cell Biol. *155*, 979–990.

Hubbs, A. E., Majidi, M., and Lichy, J. H. (1999). Expression of an isoform of the novel signal transduction protein ST5 is linked to cell morphology. Oncogene *18*, 2519–2525.

Imai, J., Toh-E, A., and Matsui, Y. (1996). Genetic analysis of the *Saccharomyces cerevisiae* RH03 gene, encoding a Rho-type small GTPase, provides evidence for a role in bud formation. Genetics *142*, 359–369.

Ito, T., Chiba, T., Ozawa, R., Yoshida, M., Hattori, M., and Sakaki, Y. (2001). A comprehensive two-hybrid analysis to explore the yeast protein interactome. Proc. Natl. Acad. Sci. USA *98*, 4569–4574.

Iwasaki, K., Staunton, J., Saifee, O., Nonet, M., and Thomas, J. H. (1997). aex-3 encodes a novel regulator of presynaptic activity in *C. elegans.* Neuron *18*, 613–622.

Jones, D. T. (1999). Protein secondary structure prediction based on position-specific scoring matrices. J. Mol. Biol. *292*, 195–202.

Karplus, K., Barrett, C., and Hughey, R. (1998). Hidden Markov models for detecting remote protein homologies. Bioinformatics *14*, 846–856.

Karplus, K., Karchin, R., Draper, J., Casper, J., Mandel-Gutfreund, Y., Diekhans, M., and Hughey, R. (2003). Combining local-structure, fold-recognition, and new fold methods for protein structure prediction. Proteins *53*(Suppl 6), 491–496.

Karpova, T. S., Moltz, S. L., Riles, L. E., Guldener, U., Hegemann, J. H., Veronneau, S., Bussey, H., and Cooper, J. A. (1998). Depolarization of the actin cytoskeleton is a specific phenotype in *Saccharomyces cerevisiae.* J. Cell Sci. *111*(Pt 17), 2689–2696.

Karpova, T. S., Reck-Peterson, S. L., Elkind, N. B., Mooseker, M. S., Novick, P. J., and Cooper, J. A. (2000). Role of actin and Myo2p in polarized secretion and growth of *Saccharomyces cerevisiae.* Mol. Biol. Cell *11*, 1727–1737.

Katzmann, D. J., Stefan, C. J., Babst, M., and Emr, S. D. (2003). Vps27 recruits ESCRT machinery to endosomes during MVB sorting. J. Cell Biol. *162*, 413–423.

Kessels, M. M., Dong, J., Leibig, W., Westermann, P., and Qualmann, B. (2006). Complexes of syndapin II with dynamin II promote vesicle formation at the trans-Golgi network. J. Cell Sci. *119*, 1504–1516.

Kim, D. E., Chivian, D., and Baker, D. (2004). Protein structure prediction and analysis using the Robetta server. Nucleic Acids Res. *32*, W526–W531.

Kirchhausen, T. (2000). Clathrin. Annu. Rev. Biochem. *69*, 699–727.

Koshland, D., Kent, J. C., and Hartwell, L. H. (1985). Genetic analysis of the mitotic transmission of minichromosomes. Cell *40*, 393–403.

Kroschewski, R., Hall, A., and Mellman, I. (1999). Cdc42 controls secretory and endocytic transport to the basolateral plasma membrane of MDCK cells. Nat. Cell Biol. *1*, 8–13.

Laemmli, U. K. (1970). Cleavage of structural proteins during the assembly of the head of bacteriophage T4. Nature *227*, 680–685.

Lee, M. C., Miller, E. A., Goldberg, J., Orci, L., and Schekman, R. (2004). Bi-directional protein transport between the ER and Golgi. Annu. Rev. Cell. Dev. Biol. *20*, 87–123.

Lee, N. K., and Lee, S. Y. (2002). Modulation of life and death by the tumor necrosis factor receptor-associated factors (TRAFs). J. Biochem. Mol. Biol. *35*, 61–66.

Letunic, I., Copley, R. R., Schmidt, S., Ciccarelli, F. D., Doerks, T., Schultz, J., Ponting, C. P., and Bork, P. (2004). SMART 4.0, towards genomic data integration. Nucleic Acids Res. *32*, D142–D144.

Levivier, E., Goud, B., Souchet, M., Calmels, T. P., Mornon, J. P., and Callebaut, I. (2001). uDENN, DENN, and dDENN: indissociable domains in Rab and MAP kinases signaling pathways. Biochem. Biophys. Res. Commun. *287*, 688–695.

Liljedahl, M., Maeda, Y., Colanzi, A., Ayala, I., Van, L. J., and Malhotra, V. (2001). Protein kinase D regulates the fission of cell surface destined transport carriers from the trans-Golgi network. Cell *104*, 409–420.

Litvak, V., Dahan, N., Ramachandran, S., Sabanay, H., and Lev, S. (2005). Maintenance of the diacylglycerol level in the Golgi apparatus by the Nir2 protein is critical for Golgi secretory function. Nat. Cell Biol. *7*, 225–234.

Liu, H., Krizek, J., and Bretscher, A. (1992). Construction of a GAL1-regulated yeast cDNA expression library and its application to the identification of genes whose overexpression causes lethality in yeast. Genetics *132*, 665–673.

Majidi, M., Gutkind, J. S., and Lichy, J. H. (2000). Deletion of the COOH terminus converts the ST5 p70 protein from an inhibitor of RAS signaling to an activator with transforming activity in NIH-3T3 cells. J. Biol. Chem. *275*, 6560–6565.

Matsui, Y., and Toh-E, A. (1992a). Isolation and characterization of two novel Ras superfamily genes in *Saccharomyces cerevisiae.* Gene (Amsterdam) *114*, 43–49.

Matsui, Y., and Toh-E, A. (1992b). Yeast RHO3 and RHO4 ras superfamily genes are necessary for bud growth, and their defect is suppressed by a high dose of bud formation genes CDC42 and BEM1. Mol. Cell. Biol. *12*, 5690–5699.

McDermott, M., Wakelam, M. J., and Morris, A. J. (2004). Phospholipase D. Biochem. Cell Biol. *82*, 225–253.

McGuffin, L. J., Bryson, K., and Jones, D. T. (2000). The PSIPRED protein structure prediction server. Bioinformatics *16*, 404–405.

Mizuta, K., and Warner, J. R. (1994). Continued functioning of the secretory pathway is essential for ribosome synthesis. Mol. Cell. Biol. *14*, 2493–2502.

Mortimer, R. K., and Johnston, J. R. (1986). Genealogy of principal strains of the yeast genetic stock center. Genetics *113*, 35–43.

Mulherkar, N., Ramaswamy, M., Mordi, D. C., and Prabhakar, B. S. (2006). MADD/DENN splice variant of the IG20 gene is necessary and sufficient for cancer cell survival. Oncogene *25*, 6252–6261.

Müsch, A., Cohen, D., Kreitzer, G., and Rodriguez-Boulan, E. (2001). cdc42 regulates the exit of apical and basolateral proteins from the trans-Golgi network. EMBO J. *20*, 2171–2179.

Natarajan, P., Wang, J., Hua, Z., and Graham, T. R. (2004). Drs2p-coupled aminophospholipid translocase activity in yeast Golgi membranes and relationship to in vivo function. Proc. Nat. Acad. Sci. USA *101*, 10614–10619.

Nie, Z., Hirsch, D. S., and Randazzo, P. A. (2003). Arf and its many interactors. Curr. Opin. Cell Biol. *15*, 396–404.

Notredame, C., Higgins, D. G., and Heringa, J. (2000). T-Coffee: a novel method for fast and accurate multiple sequence alignment. J. Mol. Biol. *302*, 205–217.

Novick, P., and Botstein, D. (1985). Phenotypic analysis of temperature-sensitive yeast actin mutants. Cell *40*, 405–416.

Novick, P., Field, C., and Schekman, R. (1980). Identification of 23 complementation groups required for post-translational events in the yeast secretory pathway. Cell *21*, 205–215.

Pearse, B.M.F., and Robinson, M. S. (1990). Clathrin, adaptors and sorting. Annu. Rev. Cell Biol. *6*, 151–171.

Pearson, C. L., Xu, K., Sharpless, K. E., and Harris, S. D. (2004). MesA, a novel fungal protein required for the stabilization of polarity axes in *Aspergillus nidulans.* Mol. Biol. Cell *15*, 3658–3672.

Peter, B. J., Kent, H. M., Mills, I. G., Vallis, Y., Butler, P.J.G., Evans, P. R., and McMahon, H. T. (2004). BAR domains as sensors of membrane curvature: the amphiphysin BAR structure. Science *303*, 495–499.

Peters, C., Baars, T. L., Buhler, S., and Mayer, A. (2004). Mutual control of membrane fission and fusion proteins. Cell *119*, 667–678.

Polishchuk, E. V., Di Pentima, A., Luini, A., and Polishchuk, R. S. (2003). Mechanism of constitutive export from the golgi: bulk flow via the formation, protrusion, and en bloc cleavage of large trans-golgi network tubular domains. Mol. Biol. Cell *14*, 4470–4485.

Polishchuk, R. S., Polishchuk, E. V., Marra, P., Alberti, S., Buccione, R., Luini, A., and Mironov, A. A. (2000). Correlative light-electron microscopy reveals the tubular-saccular ultrastructure of carriers operating between Golgi apparatus and plasma membrane. J. Cell Biol. *148*, 45–58.

Pruyne, D., Evangelista, M., Yang, C., Bi, E., Zigmond, S., Bretscher, A., and Boone, C. (2002). Role of formins in actin assembly: nucleation and barbed-end association. Science *297*, 612–615.

Pruyne, D. W., Schott, D. H., and Bretscher, A. (1998). Tropomyosin-containing actin cables direct the Myo2p-dependent polarized delivery of secretory vesicles in budding yeast. J. Cell Biol. *143*, 1931–1945.

Rambourg, A., Clermont, Y., and Kepes, F. (1993). Modulation of the Golgi apparatus in *Saccharomyces cerevisiae* sec7 mutants as seen by three-dimensional electron microscopy. Anat. Rec. *237*, 441–452.

Rambourg, A., Clermont, Y., Nicaud, J. M., Gaillardin, C., and Kepes, F. (1996). Transformations of membrane-bound organelles in sec14 mutants of the yeasts *Saccharomyces cerevisiae* and *Yarrowia lipolytica*. Anat. Rec. *245*, 448–458.

Ren, G., Vajjhala, P., Lee, J. S., Winsor, B., and Munn, A. L. (2006). The BAR domain proteins: molding membranes in fission, fusion, and phagy. Microbiol. Mol. Biol. Rev. *70*, 37–120.

Rexach, M. F., Latterich, M., and Schekman, R. (1994). Characteristics of endoplasmic reticulum-derived transport vesicles. J. Cell Biol. *126*, 1133–1148.

Reynolds, E. S. (1963). The use of lead citrate at high pH as an electron-opaque stain in electron microscopy. J. Cell Biol. *17*, 208–212.

Robinson, J. S., Klionsky, D. J., Banta, L. M., and Emr, S. D. (1988). Protein sorting in *Saccharomyces cerevisiae*: isolation of mutants defective in the delivery and processing of multiple vacuolar hydrolases. Mol. Cell. Biol. *8*, 4936–4948.

Robinson, M. S. (2004). Adaptable adaptors for coated vesicles. Trends Cell Biol. *14*, 167–174.

Rost, B., and Sander, C. (1993). Prediction of protein secondary structure at better than 70% accuracy. J. Mol. Biol. *232*, 584–599.

Roth, M. G. (2004). Phosphoinositides in constitutive membrane traffic. Physiol. Rev. *84*, 699–730.

Rothman, J. H., Raymond, C. K., Gilbert, T., O'Hara, P. J., and Stevens, T. H. (1990). A putative GTP binding protein homologous to interferon-inducible Mx proteins performs an essential function in yeast protein sorting. Cell *61*, 1063–1074.

Rothman, J. H., and Stevens, T. H. (1986). Protein sorting in yeast: mutants defective in vacuole biogenesis mislocalize vacuolar proteins into the late secretory pathway. Cell *47*, 1041–1051.

Sagot, I., Rodal, A. A., Moseley, J., Goode, B. L., and Pellman, D. (2002). An actin nucleation mechanism mediated by Bni1 and profilin. Nat. Cell Biol. *4*, 626–631.

Salminen, A., and Novick, P. (1987). A ras-like protein is required for a post-Golgi event in yeast secretion. Cell *49*, 527–538.

Sanchatjate, S., and Schekman, R. (2006). Chs5/6 Complex: a multiprotein complex that interacts with and conveys chitin synthase III from the trans-Golgi network to the cell surface. Mol. Biol. Cell *17*, 4157–4166.

Schiestl, R. H., and Gietz, R. D. (1989). High efficiency transformation of intact yeast cells using single stranded nucleic acids as a carrier. Curr. Genet. *16*, 339–346.

Schievella, A. R., Chen, J. H., Graham, J. R., and Lin, L. L. (1997). MADD, a novel death domain protein that interacts with the type 1 tumor necrosis factor receptor and activates mitogen-activated protein kinase. J. Biol. Chem. *272*, 12069–12075.

Schneider, J. C., and Guarente, L. (1991). Vectors for expressing cloned genes in yeast. Methods Enzymol. *194*, 373–388.

Schott, D. H., Collins, R. N., and Bretscher, A. (2002). Secretory vesicle transport velocity in living cells depends on the myosin-V lever arm length. J. Cell Biol. *156*, 35–39.

Sheff, D. R., Kroschewski, R., and Mellman, I. (2002). Actin dependence of polarized receptor recycling in Madin-Darby canine kidney cell endosomes. Mol. Biol. Cell *13*, 262–275.

Sherman, F. (2002). Getting started with yeast. Methods Enzymol. *350*, 3–41.

Sikorski, R. S., and Hieter, P. (1989). A system of shuttle vectors and yeast host strains designed for efficient manipulation of DNA in *Saccharomyces cerevisiae*. Genetics *122*, 19–27.

Simons, K. T., Ruczinski, I., Kooperberg, C., Fox, B. A., Bystroff, C., and Baker, D. (1999). Improved recognition of native-like protein structures using a combination of sequence-dependent and sequence-independent features of proteins. Proteins *34*, 82–95.

Simonsen, A., Wurmser, A. E., Emr, S. D., and Stenmark, H. (2001). The role of phosphoinositides in membrane transport. Curr. Opin. Cell Biol. *13*, 485–492.

Spelbrink, R. G., and Nothwehr, S. F. (1999). The yeast GRD20 gene is required for protein sorting in the trans-Golgi network/endosomal system and for polarization of the actin cytoskeleton. Mol. Biol. Cell *10*, 4263–4281.

Stechmann, A., and Cavalier-Smith, T. (2003). The root of the eukaryote tree pinpointed. Curr. Biol. *13*, R665–R666.

Stirling, C. J., Rothblatt, J., Hosobuchi, M., Deshaies, R., and Schekman, R. (1992). Protein translocation mutants defective in the insertion of integral membrane proteins into the endoplasmic reticulum. Mol. Biol. Cell *3*, 129–142.

Thompson, J. D., Higgins, D. G., and Gibson, T. J. (1994). CLUSTAL W: improving the sensitivity of progressive multiple sequence alignment through sequence weighting, position-specific gap penalties and weight matrix choice. Nucleic Acids Res. *22*, 4673–4680.

Tong, A. H. *et al.* (2004). Global mapping of the yeast genetic interaction network. Science *303*, 808–813.

Toomre, D., Keller, P., White, J., Olivo, J.-C., and Simons, K. (1999). Dual-color visualization of trans-Golgi network to plasma membrane traffic along microtubules in living cells. J. Cell Sci. *112*, 21–33.

Toyn, J. H., Gunyuzlu, P. L., White, W. H., Thompson, L. A., and Hollis, G. F. (2000). A counterselection for the tryptophan pathway in yeast: 5-fluoroanthranilic acid resistance. Yeast *16*, 553–560.

Trautwein, M., Schindler, C., Gauss, R., Dengjel, J., Hartmann, E., and Spang, A. (2006). Arf1p, Chs5p and the ChAPs are required for export of specialized cargo from the Golgi. EMBO J. *25*, 943–954.

Valdivia, R. H., Baggott, D., Chuang, J. S., and Schekman, R. W. (2002). The yeast clathrin adaptor protein complex 1 is required for the efficient retention of a subset of late Golgi membrane proteins. Dev. Cell *2*, 283–294.

Veerassamy, S., Smith, A., and Tillier, E. R. (2003). A transition probability model for amino acid substitutions from blocks. J. Comput. Biol. *10*, 997–1010.

Wada, M., Nakanishi, H., Satoh, A., Hirano, H., Obaishi, H., Matsuura, Y., and Takai, Y. (1997). Isolation and characterization of a GDP/GTP exchange protein specific for the Rab3 subfamily small G proteins. J. Biol. Chem. *272*, 3875–3878.

Walch-Solimena, C., and Novick, P. (1999). The yeast phosphatidylinositol-4-OH kinase pik1 regulates secretion at the Golgi. Nat. Cell Biol. *1*, 523–525.

Wang, C. W., Hamamoto, S., Orci, L., and Schekman, R. (2006). Exomer: a coat complex for transport of select membrane proteins from the trans-Golgi network to the plasma membrane in yeast. J. Cell Biol. *174*, 973–983.

Ward, J. J., Sodhi, J. S., McGuffin, L. J., Buxton, B. F., and Jones, D. T. (2004). Prediction and functional analysis of native disorder in proteins from the three kingdoms of life. J. Mol. Biol. *337*, 635–645.

Wedlich-Soldner, R., Altschuler, S., Wu, L., and Li, R. (2003). Spontaneous cell polarization through actomyosin-based delivery of the Cdc42 GTPase. Science *299*, 1231–1235.

Weigert, R. *et al.* (1999). CtBP/BARS induces fission of Golgi membranes by acylating lysophosphatidic acid. Nature *402*, 429–433.

Wherlock, M., Gampel, A., Futter, C., and Mellor, H. (2004). Farnesyltransferase inhibitors disrupt EGF receptor traffic through modulation of the RhoB GTPase. J. Cell Sci. *117*, 3221–3231.

Wright, R. (2000). Transmission electron microscopy of yeast. Microsc. Res. Tech. *51*, 496–510.

Wysocka, M., Bialkowska, A., Micialkiewicz, A., and Kurlandzka, A. (2003). YOR129c, a new element interacting with Cnm67p, a component of the spindle pole body of *Saccharomyces cerevisiae*. Acta Biochim. Pol. *50*, 883–890.

Yan, Q., Sun, W., Kujala, P., Lotfi, Y., Vida, T. A., and Bean, A. J. (2005). CART: an Hrs/actinin-4/BERP/myosin V protein complex required for efficient receptor recycling. Mol. Biol. Cell *16*, 2470–2482.

Yeaman, C. *et al.* (2004). Protein kinase D regulates basolateral membrane protein exit from trans-Golgi network. Nat. Cell Biol. *6*, 106–112.

Yeung, B. G., Phan, H. L., and Payne, G. S. (1999). Adaptor complex-independent clathrin function in yeast. Mol. Biol. Cell *10*, 3643–3659.

Zhang, X., Bi, E., Novick, P., Du, L., Kozminski, K. G., Lipschutz, J. H., and Guo, W. (2001). Cdc42 interacts with the exocyst and regulates polarized secretion. J. Biol. Chem. *276*, 46745–46750.

Zhang, Y., and Skolnick, J. (2004). Automated structure prediction of weakly homologous proteins on a genomic scale. Proc. Nat. Acad. Sci. USA *101*, 7594–7599.